Available online at www.sciencedirect.com
ScienceDirect
Journal of Computational Physics 223 (2007) 151–187
JOURNAL OF COMPUTATIONAL PHYSICS
www.elsevier.com/locate/jcp

Numerical resolution of a potential diphasic low Mach number system

Stéphane Dellacherie *

Commissariat à l'Énergie Atomique, DM2S-SFME, 91191 Gif sur Yvette, France
Centre de Recherches Mathématiques, Université de Montréal, C.P. 6128-succursale Centre-ville, Montréal, Que., Canada H3C 3J7

Received 6 February 2006; received in revised form 5 September 2006; accepted 7 September 2006
Available online 28 November 2006

Abstract

We propose a bidimensional algorithm for the numerical discretization of a diphasic low Mach number (DLMN) system in the case of a potential approximation, the extension to the tridimensional geometry being natural. In this algorithm, we capture the interface separating two immiscible fluids on a fixed cartesian mesh with an interface capturing algorithm. This algorithm solves a transport equation applied to an Heaviside function with a non-diffusive scheme i.e. with a scheme diffusing on a number of cells which is independent of the time integration. To take into account the artificial mixture area produced by this numerical diffusion, we have previously extended the DLMN system to the case of a mixture. Numerical results show that the algorithm is accurate and stable since the thickness of the artificial mixture area is always bounded by a constant which is of the order of the cell size, even in the case of important deformations of the interface, and since the numerical solution converges toward a good thermodynamic equilibrium with a decreasing of the entropy.

MSC: 35Q30; 65M12; 76T10; 80A10

Keywords: Diphasic flow; Low Mach number; Interface capturing; Entropy

1. Introduction

The diphasic low Mach number (DLMN) system [14,17] models non-stationary deformations of an interface separating two immiscible fluids induced by large temperature differences at low Mach number. The domain of application of the DLMN system concerns the direct numerical simulation of the diphasic flow in a nuclear reactor. Indeed, numerical simulations at the scale of bubbles coupled to experimental studies [11] may be a tool to justify average models at coarse scales.

The DLMN system is derivated in [14] and is a generalization of a system proposed by Majda in [32,33,35] which models combustion phenomena at low Mach number. In [10], it is proposed a similar model. Let us note

* Corresponding author. Tel.: +33 1 69 08 98 11; fax: +33 1 69 08 85 68.
E-mail address: stephane.dellacherie@cea.fr.

0021-9991/$ - see front matter © 2006 Elsevier Inc. All rights reserved.
doi:10.1016/j.jcp.2006.09.009

that the Majda's model is similar to the Sivashinsky's model studied in [42] (see also [39] in the case of a monophasic flow constituted of a perfect gas). The DLMN system is obtained through an asymptotic expansion applied to the diphasic compressible Navier–Stokes system which filters out the acoustic waves. This technique is identical to the one which allows to formally derive the incompressible Navier–Stokes system from the compressible Navier–Stokes system [34].

The DLMN system is an intermediate system between the diphasic compressible and incompressible Navier–Stokes systems. More exactly, the DLMN system is a *non-homogeneous* diphasic incompressible Navier–Stokes system since the divergence of the velocity field is not equal to zero because of the large temperature differences which induce compressibility effects. The DLMN system keeps the notions of equations of state and of entropy oppositely to the diphasic *incompressible* Navier–Stokes system. Nevertheless, under appropriate modelling hypothesies in one of the two fluids, the DLMN system is equal in this fluid to the incompressible Navier–Stokes system coupled to a simple heat equation [14]. An important characteristic of the DLMN system – which directly comes from the filter out of the acoustic waves – is that the thermodynamic pressure is an *average* thermodynamic pressure which does not depend on the space variable. This characteristic allows to recover *at the continuous level* some natural results concerning the dilation or the compression of a bubble at low Mach number [14]. Moreover, the DLMN system has a simple structure in monodimensional (1D) geometry since the velocity field solution of the 1D DLMN system is potential and, thus, completely decoupled from the momentum equation [14]. This property is of course also valid for the Majda's model [32,42].

On the other hand, the filter out of the acoustic waves implies that the time scale of the DLMN system is only based on the time scale associated to the fluid velocity and, thus, does not depend on the time scale associated to the acoustic waves celerity. As a consequence, the time step of any numerical discretization of the DLMN system is of the order of the time scale associated to the fluid velocity, as it is the case for the incompressible Navier–Stokes system. Oppositely, the time scale of the compressible Navier–Stokes system is based on the acoustic waves celerity at low Mach number. As a consequence, we need to solve implicitly the compressible Navier–Stokes system to have a time step based on the fluid velocity. Nevertheless, implicit compressible Navier–Stokes solvers still can be inefficient at low Mach number since the more the Mach number is low, the more the resulting linear system is ill-conditioned [37]. As a consequence, we need to use preconditioning techniques and very efficient iterative algorithms to solve such linear systems [30]. Of course, due to the elliptic part of the DLMN system, any discretization of the DLMN system implies also the resolution of a linear system. Nevertheless, the conditioning of this linear system does not depend on the Mach number.

The first theme of this paper is to study in detail numerical difficulties in a DLMN solver which may be induced by the fact that the equations of state and the thermal conductivities are not continuous functions and by the fact that the initial temperature differences are large. A possible way to study in detail such difficulties is to focus on the diphasic *thermodynamic* character rather than on the diphasic *thermodynamic* + *dynamic* character of the DLMN system by supposing that the velocity field is potential: we thus define the potential DLMN system. This hypothesis splits the momentum equation from the DLMN system which allows to eliminate the numerical difficulties coming from the dynamical character of the DLMN system. This study is important. Indeed, we will show that it may appear strong numerical instabilities when the initial temperature differences are large. For the potential DLMN system (and when the two fluids are perfect gases), we theoretically explain the origin of these numerical instabilities and we propose a cure through the notion of *entropic correction*. This correction allows to obtain an entropic property at the discrete level and is inspired from a numerical scheme solving a kinetic equation and preserving a discrete H-theorem [6,12]. We wish to underline that these instabilities would be also present in the no-potential DLMN system and that it would have been more difficult to obtain similar theoretical results in the case of this system. Let us also underline that the potential approximation of the DLMN system keeps the elliptic character of the DLMN system since the velocity field is deduced from a Poisson equation. Moreover, mathematical considerations show that the potential DLMN system should be useful to obtain existence and uniqueness results before studying the (no-potential) DLMN system [15,21,22]. Of course, we will have to couple in a future work the numerical resolution of the momentum equation to the algorithm proposed in this paper by using the approaches proposed, for example, in [7,8,26].

The second theme of that paper concerns the interface capturing algorithm. Indeed, to discretize the DLMN system in bidimensional geometry (2D), we have to transport a surface $\Sigma(t)$ defining the interface between the two immiscible fluids in a 2D bounded domain Ω. This implies that we have to develop a 2D interface *tracking* algorithm (front tracking and VOF methods enter in this class [4,23,25,27,28,45,46]) or a 2D interface *capturing* algorithm (the level set method [29,36,38,41] and the algorithm proposed in this paper enter in this class). See [45] for definitions of interface tracking and interface capturing algorithms. An interface tracking algorithm is *lagrangian* in the sense that for a front tracking algorithm, the interface $\Sigma(t)$ is explicitly represented by a connected set of points moving on the 2D mesh with the velocity flow, and in the sense that for a VOF algorithm, the interface $\Sigma(t)$ is geometrically reconstructed at each time step and propagated with a lagrangian scheme to avoid numerical smearing. At the opposite, an interface capturing algorithm is *eulerian* in the sense that the interface $\Sigma(t)$ is never explicitly represented or geometrically reconstructed. The difficulty induced by this eulerian approach is that it necessarily appears an *incertitude* on the position of $\Sigma(t)$ at each time step since we can only deduce from the eulerian algorithm that the surface $\Sigma(t)$ is inside a discretized domain $\mathscr{M}_{\Delta x}(t)$ included in Ω (Δx defining the cell size in Ω). Of course, if the numerical scheme is convergent, the more the interface capturing algorithm is accurate, the less the volume of $\mathscr{M}_{\Delta x}(t)$ is important for a given Δx. In [45], front tracking algorithms are considered to be more accurate than VOF and interface capturing algorithms. This idea comes from the fact that a front tracking algorithm represents explicitly the interface (without any geometrical reconstruction). Nevertheless, as it is underlined in [45], the major drawback of an interface tracking algorithm is its algorithmic complexity and the difficulty to take into account important topological changes of $\Sigma(t)$; moreover, additional complications arise in tridimensional geometry (3D) [45]. On the other hand, a VOF algorithm is designed to take into account important topological changes of $\Sigma(t)$ and seems to be more simple than a front tracking algorithm from an algorithmic point of view [25]. Nevertheless, a VOF algorithm includes a geometrical reconstruction algorithm which can be computationally expensive [23] and whose algorithmic complexity is more important in 3D than in 2D. At the opposite, an interface capturing algorithm takes into account topological changes without any special treatment of the algorithm and the 3D extension is natural. Thus, we think that when the topological changes are important and when the geometry is 3D, the rate *accuracy over complexity of the algorithm* of an interface capturing algorithm may be at least equal to the one of any interface tracking algorithms. Moreover, the increasing of the power of computers allows to use for 2D or 3D problems meshes finer than before.

Since the deformations of $\Sigma(t)$ modeled by the (potential or no-potential) DLMN system may be important and 3D, we choose to develop an interface capturing algorithm. To overcome the difficulty coming from the incertitude on the position of $\Sigma(t)$ induced by this eulerian approach – cf. the domain $\mathscr{M}_{\Delta x}(t)$ – and to avoid the use of any numerical tuning to keep the stability and the accuracy of the 2D scheme, we build the algorithm by following *two steps*. The first step concerns the *stability* and the *consistency* of the algorithm; the second step is related to the *accuracy* of the algorithm. These two steps are the following:

- the aim of the *first step* is to replace the previous notion of *incertitude* by the notion of *artificial mixture area*. In other words, we now consider that the domain $\mathscr{M}_{\Delta x}(t)$ defines a discretized *artificial mixture area* where the fluids 1 and 2 are mixed and, thus, where it is impossible to define any interface $\Sigma(t)$. This implies that we have to introduce *at the continuous level* a DLMN-$\mathscr{M}$ system extending the DLMN system to the case of a $\mathscr{M}$ixture. Of course, this DLMN-$\mathscr{M}$ system will have to satisfy two constraints at the continuous level (at least *formally*): the first one is that the DLMN-$\mathscr{M}$ system remains well-posed; the second one is that for any mixture domain $\mathscr{M}_{\varepsilon}(t)$ included in Ω – the variable $\varepsilon > 0$ defining the thickness of the mixture area at the continuous level – any solution of the DLMN-$\mathscr{M}$ system converges to the solution of the DLMN system in Ω when ε goes to zero. These two constraints will be (formally) satisfied by introducing appropriate closure laws at the continuous level in the mixture area $\mathscr{M}_{\varepsilon}(t)$;
- the aim of the *second step* is to control during the transient regime the volume of the domain $\mathscr{M}_{\Delta x}(t)$ by a constant $C(\Delta x)$ of the order of Δx. This property is essential since it implies that the discretized artificial mixture area $\mathscr{M}_{\Delta x}(t)$ remains always tiny compared to Ω and is uniformly controlled in time (that is to say, the constant $C(\Delta x)$ does not depend on the integration time). Thus, we can expect that the algorithm gives the *approximate* position of $\Sigma(t)$ with a high accuracy since the interface $\Sigma(t)$ is included in $\mathscr{M}_{\Delta x}(t)$. In

other words, we can say that we want to minimize the incertitude of the position of $\Sigma(t)$ during the transient regime. This second step will be achieved by transporting a Heaviside function with the non-diffusive scheme proposed by Després and Lagoutière in [18,19,31] and adapted to our context.

It is important to note that this *two-steps approach* was successfully applied by Lagoutière in [20,31] in the case of the diphasic compressible Euler system. Kokh used also the notion of artificial mixture area in [1,2,29] although the interface capturing algorithm was not based on the Després–Lagoutière's non-diffusive scheme. To our opinion, the major advantage of this *two-steps approach* is that we define a 2D algorithm in a well-defined mathematical framework in the sense that we do not use any numerical tuning to control the stability – cf. *first step* – and the accuracy – cf. *second step* – of the 2D algorithm. Thus, we think that we can be confident on the validity of the numerical results obtained in this paper. Let us also underline that the 3D extension of this 2D algorithm is natural and that the algorithmic complexity of this interface capturing algorithm is low.

It is useful to recall that the 2D interface capturing algorithm based on the *level set* approach [29,36,38,41] allows also to take into account important topological changes, the 3D extension being also natural. The basic idea of this approach comes from the fact that, at the continuous level, the position of the interface $\Sigma(t)$ can be deduced from the zero level set of any continuous function $\psi(t,x)$ advected by the velocity field. Thus, at the discretized level, the sign of the function $\psi(t,x)$ defines the two sub-domains $\Omega_1(t)$ and $\Omega_2(t)$ defining the two immiscible fluids. This interface capturing is simple. Nevertheless, for stability reasons, the sign function has to be regularized at each time step [38]. The aim of this regularization is to create at the discretized level a smooth transition area $\widehat{\mathscr{M}}_{\varepsilon}(t)$ between $\Omega_1(t)$ and $\Omega_2(t)$ whose thickness ε is also uniformly controlled. In fact, ε is of the order of Δx and is arbitrarily imposed at the beginning of the simulation (let us note that the interface tracking algorithm regularizes also the interface although the position of $\Sigma(t)$ is explicit [45]). Thus, we can think that this transition area $\widehat{\mathscr{M}}_{\varepsilon}(t)$ is similar to our artificial mixture area $\mathscr{M}_{\Delta x}(t)$. But, this is not at all the case since *the transition area $\widehat{\mathscr{M}}_{\varepsilon}(t)$ does not evolve through the discretization of a system of partial differential equations including the modeling of a transition area oppositely to the mixture area $\mathscr{M}_{\Delta x}(t)$*: the transition area $\widehat{\mathscr{M}}_{\varepsilon}(t)$ is directly created at each time step by a numerical tuning i.e. by the regularization procedure and the parameter ε. Moreover, we have to reinitialize the level set function at some regular time steps to keep a good accuracy [38] (this reinitialization keeps the function $\psi(t,x)$ close to the distance function to the interface $\Sigma(t)$). Although this reinitialization increases the accuracy of the interface capturing algorithm, it also introduces in 2D and 3D new incertitudes on the position of the interface $\Sigma(t)$, incertitudes that can be controlled with again another numerical tuning [40]. At last, although this 2D algorithm is as simple as our 2D algorithm (if we forget that it uses numerical tunings), it seems a priori difficult to obtain an entropic property oppositely to our algorithm since the transition area $\mathscr{M}_{\Delta x}(t)$ is treated by a mixture model included in the partial differential equations.

Nevertheless, an important property of the level set approach is that it is easy to take into account surface tension phenomena modeled in the spirit of [5]. Indeed, the surface tension depends in that case on the normal $n_{\Sigma(t)}$ to the interface $\Sigma(t)$ which is directly related to the level set function $\psi(t,x)$ through the formula $n_{\Sigma(t)} = \frac{\nabla\psi(t,x)}{\|\nabla\psi(t,x)\|}|_{x\in\Sigma(t)}$. But, in our algorithm, the interface $\Sigma(t)$ is described by a discretized Heaviside function which is very sharp and not by a discretized *continuous* function $\psi(t,x)$. Thus, it would be important to study the possibility to obtain a good approximation of the normal $n_{\Sigma(t)}$ when the surface $\Sigma(t)$ is deduced from a *sharp* discretized Heaviside function. This important point is not studied in that paper.

The outline of this paper is the following:

In Section 2, we recall the diphasic low Mach number (DLMN) system introduced in [14]. Then, we generalize this system when there exists a mixture area by introducing the DLMN-$\mathscr{M}$ system and we introduce the *potential approximation* of the DLMN-$\mathscr{M}$ system.

In Section 3, we propose a numerical scheme on a 2D cartesian mesh for the resolution of the potential DLMN-$\mathscr{M}$ system. Firstly, we introduce the entropic correction and we prove in a simple case that the scheme satisfies an entropic property when we correct the numerical thermal fluxes with this correction. Secondly, we describe the 2D interface capturing algorithm by adapting to our context the Després–Lagoutière's non-diffusive scheme proposed in [18,19,31]. Let us underline that this interface capturing algorithm does not depend on the potential character of the DLMN system discretized in this paper and, thus, could be also applied for the discretization of the (no-potential) DLMN system.

In Section 4, we firstly show that the 2D interface capturing algorithm is accurate by solving the 2D nonlinear hyperbolic-elliptic system proposed in [15]. This system is interesting to test the accuracy of any (2D or 3D) interface tracking or interface capturing algorithm since it can model strong vibrations of any surface $\Sigma(t)$ and since the volume $\mathscr{V}(t)$ bounded by $\Sigma(t)$ is also solution of an ordinary differential equation which can be solved explicitly. Moreover, the mathematical structure of this system is similar to the mathematical structure of the potential DLMN-$\mathscr{M}$ system. Secondly, we numerically show that the 2D algorithm solving the potential DLMN-$\mathscr{M}$ system is stable and accurate in the case of perfect gases, the thickness of the artificial mixture area being almost constant and lower than three cells, and the numerical solution converging toward a good thermodynamic equilibrium. The numerical results show also that the entropic correction is necessary at least for the proposed test cases.

2. The DLMN system

We recall in Section 2.1 the DLMN system and two important lemmas associated to this system. The details of the derivation of the DLMN system from the diphasic compressible Navier–Stokes system are written in [14]. Then, we extend in Section 2.3 this DLMN system and these two lemmas to the case of a diphasic mixture. This extension is important for the derivation of the 2D numerical algorithm in Section 3 even if we focus in that paper on the case of two *immiscible* fluids: see the *two-steps approach* presented in Section 1. At last, we introduce in Section 2.4 the *potential* approximation of the DLMN system. This approximation – which comes from an operators splitting – allows to focus on the diphasic *thermodynamic* character rather than on the diphasic *thermodynamic* + *dynamic* character of the DLMN system.

2.1. The DLMN system in the case of two immiscible fluids

The DLMN system is written in the case of two immiscible fluids. It is constituted with the two coupled systems

$$\begin{cases} D_t Y = 0, & \text{(a)} \\ \beta^{-1} D_t T = \dfrac{P'(t)}{P(t)} T + \dfrac{1}{\alpha P} \nabla \cdot (\lambda \nabla T) & \text{(b)} \end{cases} \tag{1}$$

and

$$\begin{cases} \nabla \cdot u = G, & \text{(a)} \\ \rho D_t u = -\nabla \Pi + \nabla \cdot \sigma - \rho g. & \text{(b)} \end{cases} \tag{2}$$

In the system (1) and (2), $t \geqslant 0$ is the time variable, $x \in \Omega$ is the space variable where Ω is a bounded lipschitzian open domain included in $\mathbb{R}^d$ ($d = 1$, 2 or 3). The operator $D_t := \partial_t + u \cdot \nabla$ is the lagrangian derivative operator. The function $G(t,x)$ is given by

$$G(t,x) = -\frac{1}{\Gamma} \cdot \frac{P'(t)}{P(t)} + \frac{\beta}{P(t)} \nabla \cdot (\lambda \nabla T) \tag{3}$$

and the thermodynamic pressure $P(t)$ is solution of the integro-differential equation

$$P'(t) = \frac{\displaystyle\int_\Omega \beta(Y,T,P) \nabla \cdot (\lambda \nabla T)\, \mathrm{d}x}{\displaystyle\int_\Omega \frac{\mathrm{d}x}{\Gamma(Y,T,P)}}. \tag{4}$$

Let us remark that Eq. (4) is equivalent to the *Neumann compatibility condition*

$$\int_\Omega G(t,x)\, \mathrm{d}x = 0. \tag{5}$$

The relation (5) is important to obtain the unicity of a solution of the DLMN system.

The functions $\alpha(Y,T,P)$, $\beta(Y,T,P)$ and $\Gamma(Y,T,P)$ will be defined below in each fluid k with (12): they characterize the thermodynamic properties of the diphasic flow. For example, when the fluid k is a perfect gas

whose γ-constant is equal to γ_k, these functions are respectively equal in the fluid k to $1/T$, $(\gamma_k - 1)/\gamma_k$ and γ_k (see Section 4.2). The vector $g = 9.81\hat{z}\ \mathrm{m\ s^{-2}}$ is the gravity ($\hat{z}$ is the unitary vector in the vertical direction) and $\lambda(Y,T,P)$ is the thermal conductivity. The quantities $\rho(Y,T,P)$, T, P, Π and u are, respectively, the density, the temperature, the *thermodynamic* pressure, the *dynamic* pressure and the fluid velocity. The viscosity tensor σ is defined with the Newton law

$$\sigma = \mu \cdot \left[\nabla u + (\nabla u)^t - \frac{2}{3}(\nabla \cdot u)I\right] \tag{6}$$

(I is the $d \times d$ unitary matrix) where $\mu(Y,T,P)$ is the fluid viscosity. The function $Y(t,x)$ takes its values in $\{0,1\}$ knowing that the initial condition $Y(t=0,x)$ is given by

$$Y(t=0,x) = \begin{cases} 1 & \text{if } x \in \Omega_1\ (t=0) \quad \text{(i.e. fluid 1)}, \\ 0 & \text{if } x \in \Omega_2\ (t=0) \quad \text{(i.e. fluid 2)}, \end{cases} \tag{7}$$

$\Omega_k(t=0) \neq \emptyset$ defining the initial topology of the diphasic flow ($k \in \{1,2\}$). Let us remark that (1)(a) and (7) impose that for any $(t,x) \in \mathbb{R}^+ \times \Omega$, $Y(t,x) \in \{0,1\}$. Thus, we can define the two domains $\Omega_1(t)$ and $\Omega_2(t)$ at any time $t \geqslant 0$ with $\Omega_1(t) = \{x \in \Omega \text{ such that } Y(t,x) = 1\}$ and $\Omega_2(t) = \{x \in \Omega \text{ such that } Y(t,x) = 0\}$. The function $Y(t,x)$ can be seen as the *color function* of the fluid 1 whose *discontinuity surface* $\Sigma(t) = \partial\Omega_1(t) \cap \partial\Omega_2(t)$ localizes at any time $t \geqslant 0$ the interface between the fluids 1 and 2 (we have $\Omega = \Omega_1(t) \cup \Omega_2(t) \cup \Sigma(t)$). The boundary conditions are defined with

$$\begin{cases} \forall x \in \partial\Omega: & u(t,x) = 0, & \text{(a)} \\ & \nabla T(t,x) \cdot n(x) = 0 & \text{(b)} \end{cases} \tag{8}$$

and with

$$\begin{cases} \forall x \in \Sigma(t): & u|_{\Sigma_1(t)} = u|_{\Sigma_2(t)}, & \text{(a)} \\ & \sigma|_{\Sigma_1(t)} \cdot n_{1\to 2} = \sigma|_{\Sigma_2(t)} \cdot n_{1\to 2}, & \text{(b)} \\ & T|_{\Sigma_1(t)} = T|_{\Sigma_2(t)}, & \text{(c)} \\ & \lambda\nabla T|_{\Sigma_1(t)} \cdot n_{1\to 2} = \lambda\nabla T|_{\Sigma_2(t)} \cdot n_{1\to 2}. & \text{(d)} \end{cases} \tag{9}$$

The notation $\phi|_{\Sigma_k(t)}$ corresponds to the extension on the surface $\Sigma(t)$ of the restriction of the function $\phi(t,x)$ to the open domain $\Omega_k(t)$. The vector $n_{1\to 2}$ is the unitary normal vector to the surface $\Sigma(t)$ exterior to Ω_1. The vector n is the unitary normal vector to the surface $\partial\Omega$ exterior to Ω. Let us note that under the boundary condition (8)(b), Eq. (4) is equivalent to the equation

$$P'(t) = \frac{\displaystyle\int_{\Sigma(t)} [\beta]_{\Sigma(t)}(T,P)\lambda\nabla T \cdot n_{1\to 2}\, \mathrm{d}\Sigma}{\displaystyle\int_\Omega \frac{\mathrm{d}x}{\Gamma(Y,T,P)}} - \frac{\displaystyle\int_\Omega \frac{\partial\beta}{\partial T}(Y,T,P)\lambda(Y,T,P)(\nabla T)^2\, \mathrm{d}x}{\displaystyle\int_\Omega \frac{\mathrm{d}x}{\Gamma(Y,T,P)}} \tag{10}$$

with $[\beta]_\Sigma(T,P) := \beta_1(T,P)|_\Sigma - \beta_2(T,P)|_\Sigma$. The first term in the right-hand side of (10) is due to the discontinuity of the equations of state at the interface $\Sigma(t)$; the second term is equal to zero when the two fluids are perfect gases (β is a constant in that case: see Section 4.2).

The system (1) is a mixed hyperbolic + "parabolic" system and the system (2) is a non-homogeneous diphasic incompressible Navier–Stokes system. To close the system (1)–(9), it remains to define the functions $\lambda(Y,T,P)$, $\mu(Y,T,P)$, $\rho(Y,T,P)$, $\alpha(Y,T,P)$, $\beta(Y,T,P)$, $\Gamma(Y,T,P)$. *Because of the immiscible character of the diphasic flow*, all these functions are deduced from the simple formula

$$\begin{cases} \xi(Y,T,P) = Y\xi_1(T,P) + (1-Y)\xi_2(T,P), \\ \xi \in \{\lambda,\mu,\rho,\alpha,\beta,\Gamma\}, \\ Y \in \{0,1\}. \end{cases} \tag{11}$$

The functions λ_k (conductivity) and μ_k (viscosity) characterize the transport properties of each fluid k; the functions α_k, β_k and Γ_k characterize the thermodynamic properties of each fluid k and are defined with the formulas

$$\begin{cases} \alpha_k(T,P) = -\dfrac{1}{\rho_k}\cdot\dfrac{\partial\rho_k}{\partial T}(T,P), & \text{(a)} \\ \beta_k(T,P) = \dfrac{\alpha_k P}{\rho_k C_{\mathrm{p},k}}(T,P), & \text{(b)} \\ \Gamma_k(T,P) = \dfrac{\rho_k c_k^2}{P}(T,P). & \text{(c)} \end{cases} \tag{12}$$

The function $\alpha_k(T,P)$ is the compressibility coefficient at constant pressure of the fluid k (also called thermal or volumic expansion coefficient); the functions β_k and Γ_k are dimensionless functions. The calorific capacity at constant pressure $C_{\mathrm{p},k}(T,P)$ and the sound velocity $c_k(T,P)$ are given by

$$\begin{cases} C_{\mathrm{p},k}(T,P) = \dfrac{\partial h_k}{\partial T}(T,P), & \text{(a)} \\ c_k(T,P) = \sqrt{\dfrac{\partial\rho_k}{\partial P} - \dfrac{\alpha_k^2 T}{C_{\mathrm{p},k}}}^{-1}(T,P) & \text{(b)} \end{cases} \tag{13}$$

where $h_k := \varepsilon_k + P/\rho_k$ is the enthalpy, $\varepsilon_k(T,P)$ being the internal energy of the fluid k. The functions $\rho_k(T,P)$ and $\varepsilon_k(T,P)$ are the equations of state of the fluid k. Thus, the DLMN system (1)–(13) is closed as soon as we know analytically or experimentally the four functions $\lambda_k(T,P)$, $\mu_k(T,P)$, $\rho_k(T,P)$ and $\varepsilon_k(T,P)$.

Let us underline that Y, T, u, P and Π are the five unknowns of the five Eqs. (1)–(4). The functions $\xi(Y,T,P)$ where $\xi \in \{\lambda,\mu,\rho,\alpha,\beta,\Gamma\}$ can be considered as physical parameters depending on the unknown (Y,T,P) through the formula (11), the functions $\xi_k(T,P)$, $k \in \{1,2\}$ being given functions characterizing the physical properties of each fluid k.

2.2. Thermodynamic hypothesis and properties of the DLMN system

It is important to note that the system

$$\begin{cases} \beta^{-1} D_t T = \dfrac{P'(t)}{P(t)} T + \dfrac{1}{\alpha P}\nabla\cdot(\lambda\nabla T), & \text{(a)} \\ \nabla\cdot u = G & \text{(b)} \end{cases} \tag{14}$$

(cf. Eqs. (1)(b) and (2)(a) of the DLMN system) and the system

$$\begin{cases} \partial_t(\rho\varepsilon) + \nabla\cdot(\rho\varepsilon) = -P(t)\nabla\cdot u + \nabla\cdot(\lambda\nabla T), & \text{(a)} \\ \partial_t\rho + \nabla\cdot(\rho u) = 0, & \text{(b)} \end{cases} \tag{15}$$

where $\varepsilon(Y,T,P)$ is defined with (11) are equivalent under the thermodynamic hypothesis:

Hypothesis 2.1. The equations of state $\tau_k(T,P) := 1/\rho_k(T,P)$ and $\varepsilon_k(T,P)$ of each fluid $k \in \{1,2\}$ are such that there exists a function $s_k(\tau_k,\varepsilon_k)$ verifying

$$\begin{cases} s_k(\tau_k,\varepsilon_k) \text{ is a strictly convex function}, & \text{(a)} \\ -T\,\mathrm{d}s_k = \mathrm{d}\varepsilon_k + P\,\mathrm{d}\tau_k. & \text{(b)} \end{cases} \tag{16}$$

The function $s_k(\tau_k,\varepsilon_k)$ is the classical thermodynamic entropy of the fluid k. A direct consequence of the equivalence between the systems (14) and (15) is the following lemma:

Lemma 2.1. *Under the thermodynamic Hypothesis 2.1, the DLMN system verifies*

$$\begin{cases} \dfrac{\mathrm{d}}{\mathrm{d}t}\displaystyle\int_{\Omega_k(t)} \rho_k(T,P)(t,x)\,\mathrm{d}x = 0 \quad \textit{for } k \in \{1,2\}, & (a) \\ \dfrac{\mathrm{d}}{\mathrm{d}t}\displaystyle\int_{\Omega} \rho\varepsilon(Y,T,P)(t,x)\,\mathrm{d}x = 0, & (b) \end{cases} \tag{17}$$

where $\varepsilon(Y,T,P)$ is defined with (11).

Moreover, the DLMN system verifies also the entropic property:

Lemma 2.2. *Under the thermodynamic Hypothesis 2.1, the DLMN system verifies*

$$\frac{\mathrm{d}}{\mathrm{d}t}\mathscr{S}(Y,T,P)(t) \leqslant 0$$

where the total entropy $\mathscr{S}(Y,T,P)$ is defined with

$$\mathscr{S}(Y,T,P)(t) = \int_\Omega \rho s(Y,T,P)(t,x)\,\mathrm{d}x \tag{18}$$

knowing that the entropy $s(Y,T,P)$ is given by the formula (11). And, any equilibrium characterized by the equilibrium interface Σ^∞ – i.e. by the equilibrium color function Y^∞ – is a solution of the minimization problem

$$\mathscr{S}(Y^\infty,T^\infty,P^\infty) = \min_{T(x),P} \mathscr{S}(Y^\infty,T,P) \tag{19}$$

under the constraints

$$\begin{cases} \displaystyle\int_{\Omega_k} \rho_k(T,P)(x)\,\mathrm{d}x = \mathscr{M}_k \qquad \text{for } k\in\{1,2\}, & (a)\\ \displaystyle\int_\Omega \rho\varepsilon(Y,T,P)(x)\,\mathrm{d}x = \mathscr{E}, & (b)\\ T(x)>0 \text{ and } P>0, & (c)\\ \Omega_k \text{ such that } \partial\Omega_1\cap\partial\Omega_2 = \Sigma^\infty, & (d) \end{cases} \tag{20}$$

$\mathscr{M}_k$ and $\mathscr{E}$ being strictly positive constants defined by the initial conditions. Moreover, the equilibrium $(T^\infty(x),P^\infty)$ is unique and $T^\infty(x)$ is a strictly positive constant T^∞.

These two lemmas are important since they allow to obtain (at least formally) that the DLMN system (1)–(13) is asymptotically stable when the time t goes to infinity which means that $(T,P)(t,x)$ goes to a well defined and stable equilibrium $(T^\infty(x)=T^\infty>0, P^\infty>0)$ when $t\to+\infty$. Let us note that the thermodynamic Hypothesis 2.1 is a sufficient condition to prove that the sound velocity $c_k(T,P)$ given by (13)(b) is well defined: in other words, the quantity $\frac{\partial\rho_k}{\partial P} - \frac{\alpha_k^2 T}{C_{\mathrm{p},k}}$ is strictly positive when (16) is verified. This property is a consequence of the Godunov–Mock theorem [24] (indeed, the compressible Euler system is hyperbolic under the Hypothesis 2.1). We wish to underline that without the thermodynamic Hypothesis 2.1, the system (15) is not a priori equivalent to (14). But, the system (15) is always (formally) equivalent to the system

$$\begin{cases} \widehat{\beta}^{-1} D_t T = \dfrac{P'(t)}{P(t)} T + \dfrac{1}{\widehat{\alpha} P}\nabla\cdot(\lambda\nabla T), & \text{(a)}\\ \nabla\cdot u = -\dfrac{1}{\widehat{\Gamma}}\cdot\dfrac{P'(t)}{P(t)} + \dfrac{\beta}{P(t)}\nabla\cdot(\lambda\nabla T). & \text{(b)} \end{cases} \tag{21}$$

In this system, $\widehat{\alpha}(Y,T,P)$, $\widehat{\beta}(Y,T,P)$ and $\widehat{\Gamma}(Y,T,P)$ are still given by (11). But, $\widehat{\alpha}_k(T,P)$, $\widehat{\beta}_k(T,P)$ and $\widehat{\Gamma}_k(T,P)$ are now given by

$$\begin{cases} \widehat{\alpha}_k(T,P) = \dfrac{1-\rho_k\frac{\partial h_k}{\partial P}}{T}(T,P), & \text{(a)}\\ \widehat{\beta}_k(T,P) = \dfrac{\widehat{\alpha}_k P}{\rho_k C_{\mathrm{p},k}}(T,P), & \text{(b)}\\ \widehat{\Gamma}_k(T,P) = \dfrac{\rho_k \widehat{c}_k^2}{P}(T,P) & \text{(c)} \end{cases} \tag{22}$$

with the sound velocity $\widehat{c}_k(T,P) = \sqrt{\frac{\partial\rho_k}{\partial P} - \frac{\alpha_k\widehat{\alpha}_k T}{C_{\mathrm{p},k}}}^{-1}(T,P)$ (the function $\beta(Y,T,P)$ in (21)(b) is again defined with (11) and (12)). Thus, the system (21) allows to define a DLMN system which verifies Lemma 2.1 without the thermodynamic Hypothesis 2.1. Nevertheless, this DLMN system does not verified a priori any lemma similar to Lemma 2.2. We recall that Lemma 2.2 is essential to obtain a stable equilibrium when $t\to+\infty$. We have numerically shown in [14] that the DLMN system may be ill-posed when the thermodynamic Hypothesis 2.1 is not satisfied. Thus, in that paper, we will always suppose that the thermodynamic Hypothesis 2.1 is satisfied. Of course, under the thermodynamic Hypothesis 2.1, we can prove that formulas (12)(a) and (22)(a) are equivalent which implies that the systems (14) and (21) are equivalent in that case.

2.3. Extension in the case of a mixture: the DLMN-$\mathscr{M}$ system

In this subsection, we extend the DLMN system defined with (1)–(13) *when there exists a mixture area* i.e. when the function $Y(t,x)$ takes its values in $[0,1]$ and not only in $\{0,1\}$. This extension is important even if the aim of this paper is to propose a numerical scheme for the DLMN system i.e. in the case of two *immiscible* fluids. Indeed, any numerical *eulerian* scheme used to discretize the hyperbolic equation (1)(a) implies that when the initial condition $Y(t=0,x)$ takes its values in $\{0,1\}$, after one time step, the discretized function $Y(t>0,x)$ takes its values in $[0,1]$ because of the numerical diffusion (see also the *two-steps approach* detailed in Section 1). Thus, we now define the discrete domain $\mathscr{M}_{\Delta x}(t) := \{x \in \Omega \text{ where } Y(t,x) \in]0,1[\}$ where Δx characterizes the cell size in Ω. In our approach, the domain $\mathscr{M}_{\Delta x}(t)$ defines a discretized *artificial mixture area* where the "DLMN system" should be well-posed. The key point is to modify the formula (11) in such a way it is possible to obtain two lemmas equivalent to Lemmas 2.1 and 2.2 when $Y \in [0,1]$. From now, the function Y may not be seen as the color function of the fluid 1 but as the *mass fraction* of the fluid 1.

The DLMN system with a $\mathscr{M}$ixture area – the DLMN-$\mathscr{M}$ system – is defined with the Eqs. (1)–(8) and with closure laws defining the functions λ, μ, ρ, α, β and Γ when $Y \in [0,1]$. These closure laws will be a priori different from the closure laws (11)–(13).

2.3.1. Closure laws for the functions $\lambda(Y,T,P)$ and $\mu(Y,T,P)$

The physical coefficients $\lambda(Y,T,P)$ and $\mu(Y,T,P)$ are defined with the formula

$$\begin{cases} \xi(Y,T,P) = Y\xi_1(T,P) + (1-Y)\xi_2(T,P) & \text{if } Y \in \{0,1\}, \quad \text{(a)} \\ \xi(Y,T,P) \in [\min(\xi_1(T,P),\xi_2(T,P)), \max(\xi_1(T,P),\xi_2(T,P))] & \text{if } Y \in]0,1[, \quad \text{(b)} \\ \xi(Y,T,P) \text{ is a regular function with respect to } Y \in [0,1], & \text{(c)} \\ \xi \in \{\lambda,\mu\}. & \text{(d)} \end{cases} \tag{23}$$

As soon as the functions $x \mapsto T(t,x)$ and $x \mapsto u(t,x)$ solution of the DLMN-$\mathscr{M}$ system are $C^2(\Omega)$ functions, this formula allows to formally recover the boundary condition (9) on the interface $\Sigma(t)$ when the volume of the mixture area goes to zero. Of course, for numerical applications, we have to precise the formula (23)(b). Let us just note that among many possibilities, the two formulas

$$\xi(Y,T,P) = Y\xi_1(T,P) + (1-Y)\xi_2(T,P) \quad \text{for any } Y \in [0,1] \tag{24}$$

and

$$\frac{1}{\xi(Y,T,P)} = \frac{Y}{\xi_1(T,P)} + \frac{(1-Y)}{\xi_2(T,P)} \quad \text{for any } Y \in [0,1] \tag{25}$$

are compatible with (23). In that paper, we do not discuss on the best formulas defining λ and μ in the discretized mixture area when $\xi_1 \gg \xi_2$ for example. In Section 4, we will choose (ξ_1,ξ_2) such that $\mathscr{O}(\xi_1) = \mathscr{O}(\xi_2)$. In that case, all formulas compatible with (23) are equivalent. For sake of simplicity, we will use the formula (24) in Section 4.

2.3.2. Closure laws for the thermodynamic functions ρ, α, β and Γ

We replace the formulas (11)–(13) with

$$\begin{cases} \alpha(Y,T,P) = -\dfrac{1}{\rho}\cdot\dfrac{\partial\rho}{\partial T}(Y,T,P), & \text{(a)} \\ \beta(Y,T,P) = \dfrac{\alpha P}{\rho C_p}(Y,T,P), & \text{(b)} \\ \Gamma(Y,T,P) = \dfrac{\rho c^2}{P}(Y,T,P), & \text{(c)} \end{cases} \tag{26}$$

where

$$\begin{cases} C_{\mathrm{p}}(Y,T,P) = \dfrac{\partial h}{\partial T}(Y,T,P), & \text{(a)} \\ c(Y,T,P) = \sqrt{\dfrac{\partial \rho}{\partial P} - \dfrac{\alpha^2 T}{C_{\mathrm{p}}}}^{-1}(Y,T,P) & \text{(b)} \end{cases} \tag{27}$$

with $h := \varepsilon + P/\rho$. The functions $\rho(Y,T,P) := 1/\tau(Y,T,P)$ and $\varepsilon(Y,T,P)$ are given through the closure law

$$\begin{cases} \tau(Y,T,P) = Y\tau_1(T,P) + (1-Y)\tau_2(T,P), & \text{(a)} \\ \varepsilon(Y,T,P) = Y\varepsilon_1(T,P) + (1-Y)\varepsilon_2(T,P). & \text{(b)} \end{cases} \tag{28}$$

The functions $\rho(Y,T,P)$ and $\varepsilon(Y,T,P)$ define the *mixture equations of state*. Let us recall that $\tau_k(T,P) := 1/\rho_k(T,P)$ and $\varepsilon_k(T,P)(T,P)$ are given functions.

Thus, the DLMN-$\mathscr{M}$ system – which corresponds to the system (1)–(8) + (23)–(28) – is now closed. Let us note that the Neumann compatibility condition (5) is again valid and equivalent to (4).

2.3.3. Some remarks on the closure laws (26)–(28)

Having before defined the functions α_k, β_k and Γ_k with (12) and (13), it is natural to define α, β and Γ with the formulas (26) and (27) in the mixture area. Nevertheless, it is important to note that the formulas (26)–(28) are *only* equivalent to the formulas (11)–(13) when $Y \in \{0,1\}$ i.e. when there is no mixture area. In other words, the DLMN and DLMN-$\mathscr{M}$ systems are equivalent when the mixture area does not exist. This property is of course necessary to obtain the convergence of the solution of the DLMN-$\mathscr{M}$ system toward the solution of the DLMN system when the volume of the mixture area goes to zero (this corresponds to the consistency property of the first step of the *two-steps approach* exposed in Section 1).

Moreover, we easily deduce from the closure law (28) that the formulas (26)(a) and (27)(a) are equivalent to the formulas

$$\begin{cases} \alpha(Y,T,P) = z(Y,T,P)\alpha_1(T,P) + [1-z(Y,T,P)]\alpha_2(T,P), & \text{(a)} \\ C_{\mathrm{p}}(Y,T,P) = YC_{\mathrm{p},1}(T,P) + (1-Y)C_{\mathrm{p},2}(T,P) & \text{(b)} \end{cases} \tag{29}$$

when $Y \in [0,1]$, z being the *volumic fraction* of the fluid 1 defined with $z(Y,T,P) = Y\frac{\tau_1(T,P)}{\tau(T,P)}$. The equation (29)(b) is obtained by noting that $h := \varepsilon + P/\rho$ and (28) imply that $h = Yh_1 + (1-Y)h_2$.

The formulas (28) are classical closure laws used to close the diphasic compressible Euler system [13,31]. The closure law (28)(a) corresponds to the hypothesis that in the mixture area, the two fluids are immiscible although we do not have any information on the exact position of the interface $\Sigma(t)$ (see the introduction in [31]): in other words, the closure law (28)(a) is a *basic* homogeneization formula. The closure law (28)(b) is linked to the extensive character of the internal energy. At last, we suppose in (28) that each fluid k has the same thermodynamic pressure and temperature in the mixture. To summarize, the closure law (28) corresponds to the *isobar-isotherm* closure law applied to an homogeneized mixture of two immiscible fluids. Although we could *a priori* closed the DLMN-$\mathscr{M}$ system with other closure laws, this isobar-isotherm hypothesis seems to us natural since the DLMN system is such that the thermodynamic pressure P does not depend on the space variable and such that the temperature T is a continuous function at the interface $\Sigma(t)$ (cf. (9)(c)).

2.3.4. Basic properties of the DLMN-$\mathscr{M}$ system

The main advantage of the closure law (28) comes from the following lemma [31]:

Lemma 2.3. *Under the thermodynamic Hypothesis 2.1 and under the closure law (28), the mixture entropy* $s(Y,T,P) = Ys_1(T,P) + (1-Y)s_2(T,P)$ *can also be seen as a function of* (Y,τ,ε) *verifying*

$$\begin{cases} s(Y,\tau,\varepsilon) \text{ is a strictly convex function of } (\tau,\varepsilon), & (a) \\ -T\,\mathrm{d}s = \mathrm{d}\varepsilon + P\,\mathrm{d}\tau \text{ when } \mathrm{d}Y = 0. & (b) \end{cases} \tag{30}$$

As in the case of the DLMN system (i.e. without mixture), this lemma allows to write that the systems (14) and (15) are equivalent. As a consequence, we obtain conservation properties which are a transposition of Lemma 2.1 to the case of the DLMN-$\mathscr{M}$ system:

Lemma 2.4. *Under the thermodynamic Hypothesis 2.1, the DLMN-$\mathscr{M}$ system verifies*

$$\begin{cases} \dfrac{\mathrm{d}}{\mathrm{d}t}\displaystyle\int_\Omega Y\rho(Y,T,P)(t,x)\,\mathrm{d}x = 0, & (a)\\ \dfrac{\mathrm{d}}{\mathrm{d}t}\displaystyle\int_\Omega (1-Y)\rho(Y,T,P)(t,x)\,\mathrm{d}x = 0, & (b)\\ \dfrac{\mathrm{d}}{\mathrm{d}t}\displaystyle\int_\Omega \rho\varepsilon(Y,T,P)(t,x)\,\mathrm{d}x = 0. & (c) \end{cases} \tag{31}$$

This lemma shows that we have again a mass conservation property for each fluid k although we have lost the interface notion in the DLMN-$\mathscr{M}$ system, this notion being hidden in the mixture closure law (28)(a).

We have also the transposition of Lemma 2.2 when there exists a mixture area:

Lemma 2.5. *Under the thermodynamic Hypothesis 2.1, the DLMN-$\mathscr{M}$ system verifies the Lemma 2.2 by replacing the constraints (20) with the constraints*

$$\begin{cases} \displaystyle\int_\Omega Y\rho(Y,T,P)(x)\,\mathrm{d}x = \mathscr{M}_1, & (a)\\ \displaystyle\int_\Omega (1-Y)\rho(Y,T,P)(x)\,\mathrm{d}x = \mathscr{M}_2, & (b)\\ \displaystyle\int_\Omega \rho\varepsilon(Y,T,P)(x)\,\mathrm{d}x = \mathscr{E}, & (c)\\ T(x) > 0 \text{ and } P > 0, & (d)\\ Y(x) = Y^\infty(x) \in [0,1]. & (e) \end{cases} \tag{32}$$

Because of relations (30), the proof of Lemma 2.5 is identical to the proof of Lemma 2.2.

Lemma 2.3 – which extends the thermodynamic Hypothesis 2.1 in the mixture area – and Lemmas 2.4 and 2.5 – which are the extensions of Lemmas 2.1 and 2.2 in the mixture area – allow to be confident on the well-posed character of the DLMN-$\mathscr{M}$ system. Let us underline that, due to Lemma 2.3, the sound velocity $c(Y,T,P)$ in the mixture area defined with (27)(b) is well defined. To obtain this result, we can use an extension of the Godunov–Mock theorem in the case of a mixture [31].

2.4. The potential DLMN-$\mathscr{M}$ system

We now define the *potential* approximation of the DLMN-$\mathscr{M}$ system by using an operators splitting. The starting point is to note that any field $u(x) \in L^2(\Omega)$ can be decomposed with

$$\begin{cases} u(x) = w(x) + \nabla\Phi(x) \text{ where } \nabla\cdot w = 0,\\ \nabla\Phi\cdot n|_{\partial\Omega} = u\cdot n|_{\partial\Omega},\\ w\cdot n|_{\partial\Omega} = 0 \end{cases} \tag{33}$$

which corresponds to the Hodge decomposition [9]. The fields w and $\nabla\Phi$ are, respectively, the solenoidal (free divergence) and potential parts of the field u. The decomposition (33) is unique (up to a constant for the potential Φ). By decomposing the velocity field $u(t,x)$ of the DLMN-$\mathscr{M}$ system with (33) and by injecting this decomposition in the system (2) and in the boundary condition (8)(a), we obtain the system

$$\begin{cases} \Delta\Phi = G, & (a)\\ \nabla\Phi\cdot n|_{\partial\Omega} = 0 & (b) \end{cases} \tag{34}$$

coupled to the *non-homogeneous* diphasic incompressible Navier–Stokes system

$$\begin{cases} \nabla\cdot w = 0, & (a)\\ \rho D_t w = -\nabla\Pi + \nabla\cdot\sigma - \rho g - \rho D_t\nabla\Phi, & (b)\\ w\cdot n|_{\partial\Omega} = 0, & (c)\\ w\cdot\tau|_{\partial\Omega} = -\nabla\Phi\cdot\tau|_{\partial\Omega} & (d) \end{cases} \tag{35}$$

where τ is the tangential vector to the boundary $\partial\Omega$ and where

$$D_t := \partial_t + (w + \nabla\Phi)\cdot\nabla.$$

Eq. (34) describes the diphasic *thermodynamic* character of the DLMN-$\mathscr{M}$ system; the system (35) describes the diphasic *dynamic* character of the DLMN-$\mathscr{M}$ system. Of course, this two characters are coupled. Let us underline that when $\nabla\Phi \equiv 0$, the system (35) coupled to (1)(a) and (11) is the diphasic incompressible Navier–Stokes system whose numerical discretization was studied with interface tracking techniques [4,23,25,27,28,45,46] or with the level set approach in [38]. To focus on numerical difficulties coming from the diphasic *thermodynamic* character of the DLMN-$\mathscr{M}$ system, we split the system (35) from the DLMN-$\mathscr{M}$ system. Thus, we suppose that:

Hypothesis 2.2. The velocity field $u(t,x)$ is potential.

This hypothesis allows to obtain the system

$$\begin{cases} D_t Y = 0, & \text{(a)} \\ \beta^{-1} D_t T = \dfrac{P'(t)}{P(t)} T + \dfrac{1}{\alpha P}\nabla\cdot(\lambda\nabla T) & \text{(b)} \end{cases} \tag{36}$$

coupled to

$$\begin{cases} \Delta\Phi = G, & \text{(a)} \\ \nabla\Phi\cdot n|_{\partial\Omega} = 0 & \text{(b)} \end{cases} \tag{37}$$

with now

$$D_t := \partial_t + \nabla\Phi\cdot\nabla$$

since $u(t,x) = \nabla\Phi(t,x)$. The system (36) and (37) defines the *potential* approximation of the DLMN-$\mathscr{M}$ system. Of course, this system is closed with Eqs. (3), (4), (8)(b) and (23)–(28). Moreover, Lemmas 2.3–2.5 are still verified. Let us remark that we can add in Lemma 2.5 *only in the case of the potential DLMN-$\mathscr{M}$ system* that $u(t,x) \to 0$ when (T,P) converges to the equilibrium (T^∞, P^∞) since $G \to 0$ coupled to (37) implies that $\nabla\Phi \to 0$.

Let us underline that the potential approximation of the DLMN-$\mathscr{M}$ *keeps the elliptic character of the DLMN system* since the velocity field is deduced from the Poisson equation (37). Moreover, any solution Φ of the elliptic equation (37) is unique (up to a constant) because of the Neumann compatibility condition (5) (cf. the Fredholm alternative). And, as soon as $x \mapsto G(t,x)$ is in $L^\infty(\Omega)$, standard elliptic regularity results show that $x \mapsto \nabla\Phi(t,x)$ is a continuous function. Thus, the velocity field $u := \nabla\Phi$ is unique and continuous.

Remark on Hypothesis 2.2

Of course, Hypothesis 2.2 is not valid from a physical point of view. Nevertheless, the splitting (34) and (35) is useful from a theoretical and numerical point of view. Indeed, this splitting is useful to obtain existence and uniqueness results for the Majda's low Mach number system [21,22,34,35]: this could be also the case for the DLMN system. More precisely, it is natural to firstly obtain existence and uniqueness results for the potential approximation of the DLMN system before studying the (no-potential) DLMN system. We think that this is also the case at the numerical point of view in the sense that any good DLMN solver will have necessarily to be a good DLMN solver in the potential case. In Sections 3 and 4, we will show that it can appear *strong* numerical instabilities when the initial temperature differences are large, and we will propose and justify a cure by studying the discretization of the potential DLMN system. These instabilities would also appear with the no-potential DLMN solver.

3. Discretization of the potential DLMN-$\mathcal{M}$ system

We now propose a 2D numerical scheme for the discretization of the potential DLMN-$\mathscr{M}$ system. For sake of simplicity, we suppose that the 2D open domain Ω is equal to $]x_{\min}, x_{\max}[\times]y_{\min}, y_{\max}[$ where $x_{\min}$, $x_{\max}$, $y_{\min}$ and $y_{\max}$ are four reals; it would be possible to define a more complicated $\partial\Omega$ but it would complicate the notations because of the boundary conditions on $\partial\Omega$. Moreover, such a rectangular domain is representative of a

section of a 2D pipe in a nuclear reactor. The time subscript is equal to n and the time step is equal to Δt. The 2D spatial mesh is supposed to be cartesian. The space and interface subscripts in the x direction are, respectively, defined with i and $i+1/2$; the same quantities are defined in the y direction by replacing i with j. The cell size is equal to Δx in the x direction and to Δy in the y direction.

The 3D extension of the 2D algorithm proposed in this section – *including the interface capturing algorithm proposed in Section 3.4* – is natural, and all the properties written in 2D are also verified for the 3D extension.

3.1. Formulation of the 2D scheme

We discretize the system (36) and (37) with

$$\begin{cases} Y_{i,j}^{n+1} = Y_{i,j}^n - \Delta t \cdot \mathscr{T}_Y(\Phi^n, Y^n)_{i,j}, & \text{(a)} \\ T_{i,j}^{n+1} = T_{i,j}^n + \Delta t \cdot \left[-\mathscr{T}_T(\Phi^n, T^n)_{i,j} + \beta_{i,j}^n \left(\dfrac{\mathscr{P}'(Y^n, T^n, P^n)}{P^n} T_{i,j}^n + \dfrac{\widehat{\mathscr{D}}_T(Y^n, T^n)_{i,j}}{\alpha_{i,j}^n P^n} \right) \right] & \text{(b)} \end{cases} \tag{38}$$

and

$$\Delta_{\Delta x,\Delta y}(\Phi^n) = G^n. \tag{39}$$

The discrete operators $\mathscr{T}_Y(\Phi, Y)$ and $\mathscr{T}_T(\Phi, T)$, respectively, discretize the continuous operators $\nabla\Phi \cdot \nabla Y$ and $\nabla\Phi \cdot \nabla T$. The discrete operator $\widehat{\mathscr{D}}_T(Y, T)$ discretizes the diffusion operator $\nabla \cdot (\lambda \nabla T)$. In (39), $\Delta_{\Delta x,\Delta y}(\Phi)$ is the classical 2D discrete laplacian operator on a 2D cartesian mesh with Neumann boundary conditions. It is defined with

$$\Delta_{\Delta x,\Delta y}(\Phi) = \frac{\Phi_{i-1,j} - 2\Phi_{i,j} + \Phi_{i+1,j}}{\Delta x^2} + \frac{\Phi_{i,j-1} - 2\Phi_{i,j} + \Phi_{i,j+1}}{\Delta y^2}$$

when the cell (i,j) does not have any interface belonging to the boundary $\partial\Omega$. When one interface belongs to $\partial\Omega$ – let us say the interface $(i-1/2,j)$ – the discrete operator $\Delta_{\Delta x,\Delta y}$ is given by

$$\Delta_{\Delta x,\Delta y}(\Phi) = \frac{-\Phi_{i,j} + \Phi_{i+1,j}}{\Delta x^2} + \frac{\Phi_{i,j-1} - 2\Phi_{i,j} + \Phi_{i,j+1}}{\Delta y^2}.$$

Let us underline that $\Delta_{\Delta x,\Delta y}$ is simple because the mesh is supposed to be cartesian. Using formula (3), we define the vector $(G_{i,j}^n)_{i,j}$ with

$$G_{i,j}^n = -\frac{1}{\Gamma_{i,j}^n} \cdot \frac{\mathscr{P}'(Y^n, T^n, P^n)}{P^n} + \frac{\beta_{i,j}^n}{P^n} \cdot \mathscr{D}_T(Y^n, T^n)_{i,j} \tag{40}$$

where $\mathscr{P}'(Y^n, T^n, P^n)$ approximates the quantity $P'(t^n)$. As $\widehat{\mathscr{D}}_T(Y, T)$, the discrete operator $\mathscr{D}_T(Y, T)$ discretizes the diffusion operator $\nabla \cdot (\lambda \nabla T)$; $\mathscr{D}_T$ and $\widehat{\mathscr{D}}_T$ are not equal for reasons which will be exposed in Section 3.3. The equation (39) – whose the unknown is the vector $(\Phi_{i,j}^n)_{i,j}$ – is solved with a conjugate gradient method or with a discrete fast Fourier transform. At last, the thermodynamic pressure is given by the scheme

$$P^{n+1} = \wp(Y^n, Y^{n+1}, T^n, T^{n+1}, P^n) \tag{41}$$

by noting that $(Y_{i,j}^{n+1})_{i,j}$ and $(T_{i,j}^{n+1})_{i,j}$ were previously computed with the explicit scheme (38) and (39). Of course, the quantity $\wp(Y^n, Y^{n+1}, T^n, T^{n+1}, P^n)$ is an estimation of $P(t^{n+1})$. Let us underline that $\alpha_{i,j}^n$, $\beta_{i,j}^n$ and $\Gamma_{i,j}^n$ are, respectively, equal to $\alpha(Y_{i,j}^n, T_{i,j}^n, P^n)$, $\beta(Y_{i,j}^n, T_{i,j}^n, P^n)$ and $\Gamma(Y_{i,j}^n, T_{i,j}^n, P^n)$, the functions $\alpha(Y,T,P)$, $\beta(Y,T,P)$ and $\Gamma(Y,T,P)$ being deduced from the *mixture equations of state* $\rho(Y,T,P)$ and $\varepsilon(Y,T,P)$ (see 26,27,29). Moreover, the conductivity $\lambda_{i,j}^n$ is equal to $\lambda(Y_{i,j}^n, T_{i,j}^n, P^n)$ where $\lambda(Y,T,P)$ is compatible with (23) ($\lambda(Y,T,P)$ may be given by (24) for example, which will be the case in Section 4).

The operators $\mathscr{P}'(Y^n, T^n, P^n)$ and $\wp(Y^n, Y^{n+1}, T^n, T^{n+1}, P^n)$ are given in Section 3.2. The operators $\mathscr{D}_T(Y, T)$, $\widehat{\mathscr{D}}_T(Y, T)$ and $\mathscr{T}_T(\Phi, T)$ are given in Section 3.3. The operator $\mathscr{T}_Y(\Phi, Y)$ is given in Section 3.4 and defines the 2D interface capturing algorithm.

3.2. The operators $\mathscr{P}'(Y^n, T^n, P^n)$ and $\wp(Y^n, Y^{n+1}, T^n, T^{n+1}, P^n)$

We firstly define the discrete operator $\mathscr{P}'(Y^n, T^n, P^n)$. Secondly, we propose three different schemes defining $\wp(Y^n, Y^{n+1}, T^n, T^{n+1}, P^n)$.

3.2.1. The operator $\mathscr{P}'(Y^n, T^n, P^n)$

We define $\mathscr{P}'(Y^n, T^n, P^n)$ with

$$\mathscr{P}'(Y^n, T^n, P^n) = \frac{\sum_{i,j} \beta^n_{i,j} \cdot \mathscr{D}_T(Y^n, T^n)_{i,j} \Delta x \, \Delta y}{\sum_{i,j} \dfrac{\Delta x \, \Delta y}{\Gamma^n_{i,j}}}. \tag{42}$$

This formula is of course consistent with (4). Moreover, (40) and (42) show that

$$\sum_{i,j} G^n_{i,j} \Delta x \, \Delta y = 0 \tag{43}$$

which is a discretized version of the Neumann compatibility condition (5). Condition (43) implies that the discrete elliptic equation (39) admits an unique solution $(\Phi^n_{i,j})_{i,j}$ up to a constant (in other words, the matrix $\Delta_{\Delta x, \Delta y}$ is invertible in the subspace orthogonal to the identity vector). Thus, the 2D discrete potential velocity field (u,v) given by

$$\begin{cases} u^n_{i+1/2,j} := \dfrac{\Phi^n_{i+1,j} - \Phi^n_{i,j}}{\Delta x}, & \text{(a)} \\ v^n_{i,j+1/2} := \dfrac{\Phi^n_{i,j+1} - \Phi^n_{i,j}}{\Delta y} & \text{(b)} \end{cases} \tag{44}$$

is well defined and satisfies the boundary condition (8)(a) on $\partial\Omega$. Let us remark that the 2D velocity field is defined on a staggered grid as in [26].

3.2.2. The operator $\wp(Y^n, Y^{n+1}, T^n, T^{n+1}, P^n)$

There are three possible numerical schemes (see also [14] in the 1D lagrangian case). The two first schemes conserve respectively the mass and the energy, and are *implicit* (except when the two fluids are perfect gases: see Section 4). The last scheme does not conserve the mass and the energy but is *explicit*.

Conservative scheme in mass:

Using Eqs. (31)(a) and (b), we can evaluate the pressure $P^{n+1} = \wp$ through one of the three non-linear equations

$$\begin{cases} \sum_{i,j} Y^{n+1}_{i,j} \rho(Y^{n+1}_{i,j}, T^{n+1}_{i,j}, \wp) \Delta x \, \Delta y = \sum_{i,j} Y^n_{i,j} \rho(Y^n_{i,j}, T^n_{i,j}, P^n) \Delta x \, \Delta y, & \text{(a)} \\ \sum_{i,j} (1 - Y^{n+1}_{i,j}) \rho(Y^{n+1}_{i,j}, T^{n+1}_{i,j}, \wp) \Delta x \, \Delta y = \sum_{i,j} (1 - Y^n_{i,j}) \rho(Y^n_{i,j}, T^n_{i,j}, P^n) \Delta x \, \Delta y, & \text{(b)} \\ \sum_{i,j} \rho(Y^{n+1}_{i,j}, T^{n+1}_{i,j}, \wp) \Delta x \, \Delta y = \sum_{i,j} \rho(Y^n_{i,j}, T^n_{i,j}, P^n) \Delta x \, \Delta y & \text{(c)} \end{cases} \tag{45}$$

as soon as $(Y, T)^{n+1}_{i,j}$ is known. The non-linear equations (45)(a), (b) or (c) implicitly define three possible operators $\wp$ with

$$P^{n+1} = \wp(Y^n, Y^{n+1}, T^n, T^{n+1}, P^n) \text{ where } \wp \text{ is the unique strictly positive solution of (45)(a), (b) or (c).} \tag{46}$$

By using Eqs. (45)(a), (b) or (c), the scheme is respectively conservative for the mass of fluid 1, for the mass of fluid 2 or for the total mass. Nevertheless, this scheme is never conservative for the mass of fluid 1 *and* for the mass of fluid 2. These three schemes do not conserve the energy.

Conservative scheme in energy:

Using the same approach, we can see that the discrete version

$$\sum_{i,j} \rho\varepsilon(Y_{i,j}^{n+1}, T_{i,j}^{n+1}, \wp)\Delta x\,\Delta y = \sum_{i,j} \rho\varepsilon(Y_{i,j}^{n}, T_{i,j}^{n}, P^{n})\Delta x\,\Delta y \tag{47}$$

of Eq. (31)(c) allows to implicitly defines another operator $\wp$ with

$$P^{n+1} = \wp(Y^n, Y^{n+1}, T^n, T^{n+1}, P^n) \text{ where } \wp \text{ is the unique strictly positive solution of the equation (47).} \tag{48}$$

This scheme is conservative in energy but does not conserve the mass of any fluid.

Non-conservative scheme in mass and in energy:

Having previously define the operator $\mathscr{P}'(Y^n, T^n, P^n)$ with (42), we can also define the explicit operator $\wp$ with

$$P^{n+1} = \wp(Y^n, Y^{n+1}, T^n, T^{n+1}, P^n) = \wp(Y^n, T^n, P^n) \text{ where } \wp(Y^n, T^n, P^n) := P^n + \Delta t \cdot \mathscr{P}'(Y^n, T^n, P^n). \tag{49}$$

The scheme (49) is explicit but cannot be conservative in mass or in energy. Moreover, the time step Δt has to verify

$$\Delta t < -\frac{P^n}{\mathscr{P}'(Y^n, T^n, P^n)} \text{ when } \mathscr{P}'(Y^n, T^n, P^n) < 0 \tag{50}$$

in such a way the pressure P^{n+1} remains strictly positive.

3.3. The operators $\mathscr{D}_T(Y,T)$, $\widehat{\mathscr{D}}_T(Y,T)$ and $\mathscr{T}_T(\Phi,T)$, and the entropic correction

We now define $\mathscr{D}_T(Y,T)$. Then, we define $\widehat{\mathscr{D}}_T(Y,T)$ and $\mathscr{T}_T(\Phi,T)$. The operator $\widehat{\mathscr{D}}_T(Y,T)$ is not equal to $\mathscr{D}_T(Y,T)$ despite $\mathscr{D}_T(Y,T)$ and $\widehat{\mathscr{D}}_T(Y,T)$ discretize the same continuous operator $\nabla\cdot(\lambda\nabla T)$. Indeed, we have to introduce an *entropic correction* in $\widehat{\mathscr{D}}_T(Y,T)$ in such a way $(T_{i,j}^n, P^n)$ converges to a good discrete equilibrium $(T_{i,j}^\infty = T^\infty > 0, P^\infty > 0)$ when n goes to infinity (see Lemma 2.5).

3.3.1. The operator $\mathscr{D}_T(Y,T)$

We define the discrete diffusion operator with the classical conservative formula

$$\mathscr{D}_T(Y,T)_{i,j} = \frac{\mathscr{F}^x_{\mathscr{D}_T}(Y,T)_{i+1/2,j} - \mathscr{F}^x_{\mathscr{D}_T}(Y,T)_{i-1/2,j}}{\Delta x} + \frac{\mathscr{F}^y_{\mathscr{D}_T}(Y,T)_{i,j+1/2} - \mathscr{F}^y_{\mathscr{D}_T}(Y,T)_{i,j-1/2}}{\Delta y} \tag{51}$$

where

$$\begin{cases} \mathscr{F}^x_{\mathscr{D}_T}(Y,T)_{i+1/2,j} = \lambda_{i+1/2,j}\cdot\dfrac{T_{i+1,j} - T_{i,j}}{\Delta x}, & \text{(a)} \\ \mathscr{F}^y_{\mathscr{D}_T}(Y,T)_{i,j+1/2} = \lambda_{i,j+1/2}\cdot\dfrac{T_{i,j+1} - T_{i,j}}{\Delta y}. & \text{(b)} \end{cases} \tag{52}$$

When the interface $(i+1/2,j)$ (or $(i,j+1/2)$) belongs to $\partial\Omega$ we impose $\mathscr{T}^x_{\mathscr{D}_T}(Y,T)_{i+1/2,j} = 0$ (or $\mathscr{T}^y_{\mathscr{D}_T}(Y,T)_{i,j+1/2} = 0$) (if the boundary condition (8)(b)). In (52), the conductivities $\lambda_{i+1/2,j}$ and $\lambda_{i,j+1/2}$ may be defined for example with the formulas

$$\begin{cases} \lambda_{i+1/2,j} = \dfrac{\lambda_{i+1,j} + \lambda_{i,j}}{2}, \\ \lambda_{i,j+1/2} = \dfrac{\lambda_{i,j+1} + \lambda_{i,j}}{2} \end{cases} \tag{53}$$

or with the formulas

$$\begin{cases} \dfrac{2}{\lambda_{i+1/2,j}} = \dfrac{1}{\lambda_{i+1,j}} + \dfrac{1}{\lambda_{i,j}}, \\ \dfrac{2}{\lambda_{i,j+1/2}} = \dfrac{1}{\lambda_{i,j+1}} + \dfrac{1}{\lambda_{i,j}}. \end{cases} \tag{54}$$

When the mixture conductivity $\lambda_{i,j} := \lambda(Y_{i,j}, T_{i,j}, P)$ is given by the formula (24) or by the formula (25), it seems to us natural to use, respectively, the formula (53) or (54). In Section 4, we use the formula (53) since we define $\lambda(Y,T,P)$ with (24). Let us underline that when $\mathcal{O}(\lambda_1(T,P)) = \mathcal{O}(\lambda_2(T,P))$ – which is the case for the numerical applications in Section 4 – all average formulas are equivalent. Nevertheless, it should not be the case when $\mathcal{O}(\lambda_1(T,P)) \gg \mathcal{O}(\lambda_2(T,P))$: this point is not studied in this paper.

3.3.2. The operators $\widehat{\mathscr{D}}_T(Y,T)$ and $\mathscr{T}_T(\Phi,T)$, and the entropic correction

Numerical results in Section 4 show that when $\widehat{\mathscr{D}}_T(Y,T) := \mathscr{D}_T(Y,T)$, the entropy $\mathscr{S}(Y^n,T^n,P^n)$ may not decrease which could imply that $(T^n_{i,j},P^n)$ does not converge toward a good equilibrium (T^∞,P^∞) when n goes to infinity: in other words, Lemma 2.5 may not be true at the discrete level when $\widehat{\mathscr{D}}_T(Y,T) := \mathscr{D}_T(Y,T)$. This means that we have to modify the formulas (51) and (52) with an *entropic correction* to define the operator $\widehat{\mathscr{D}}_T(Y,T)$ in such a way we recover the decreasing of the entropy. By studying the 2D algorithm at the semi-discrete level (i.e. continuous-in-time and discrete-in-space), we can explicit the *entropic correction* when the two fluids are perfect gases verifying $\beta_1 = \beta_2$: see Lemma 3.2. Although this *entropic correction* is obtained in a particular case, we expect that this *entropic correction* gives also good numerical results for other equations of state verifying the thermodynamic Hypothesis 2.1, especially in the case of van der Waals equations of state (which can model liquid and gas phases). Let us note that, in Section 4, we numerically show that the proposed *entropic correction* gives also good results for two perfect gases verifying $\beta_1 \neq \beta_2$.

Definition of the operators $\widehat{\mathscr{D}}_T(Y,T)$ and $\mathscr{T}_T(\Phi,T)$:

Let us define the transport operator $\mathscr{T}_T(\Phi,T)$ with the formula

$$\mathscr{T}_T(\Phi,T)_{i,j} = \mathscr{T}^x_T(\Phi,T)_{i,j} + \mathscr{T}^y_T(\Phi,T)_{i,j} \tag{55}$$

where

$$\begin{cases} \mathscr{T}^x_T(\Phi,T)_{i,j} = \dfrac{1}{2}\left[u_{i+1/2,j}\cdot\dfrac{T_{i+1,j}-T_{i,j}}{\Delta x} + u_{i-1/2,j}\cdot\dfrac{T_{i,j}-T_{i-1,j}}{\Delta x}\right], & \text{(a)} \\ \mathscr{T}^y_T(\Phi,T)_{i,j} = \dfrac{1}{2}\left[u_{i,j+1/2}\cdot\dfrac{T_{i,j+1}-T_{i,j}}{\Delta y} + u_{i,j-1/2}\cdot\dfrac{T_{i,j}-T_{i,j-1}}{\Delta y}\right] & \text{(b)} \end{cases} \tag{56}$$

knowing that the discrete velocity field is given by (44), and let us define the diffusion operator $\widehat{\mathscr{D}}_T(Y,T)$ with

$$\widehat{\mathscr{D}}_T(Y,T)_{i,j} = \frac{\widehat{\mathscr{F}}^x_{\mathscr{D}_T}(Y,T)^{i,j}_{i+1/2,j} - \widehat{\mathscr{F}}^x_{\mathscr{D}_T}(Y,T)^{i,j}_{i-1/2,j}}{\Delta x} + \frac{\widehat{\mathscr{F}}^y_{\mathscr{D}_T}(Y,T)^{i,j}_{i,j+1/2} - \widehat{\mathscr{F}}^y_{\mathscr{D}_T}(Y,T)^{i,j}_{i,j-1/2}}{\Delta y} \tag{57}$$

where

$$\begin{cases} \widehat{\mathscr{F}}^x_{\mathscr{D}_T}(Y,T)^{i,j}_{i+1/2,j} = \zeta(T)^{i,j}_{i+1/2,j}\cdot\mathscr{F}^x_{\mathscr{D}_T}(Y,T)_{i+1/2,j}, & \text{(a)} \\ \widehat{\mathscr{F}}^y_{\mathscr{D}_T}(Y,T)^{i,j}_{i,j+1/2} = \zeta(T)^{i,j}_{i,j+1/2}\cdot\mathscr{F}^y_{\mathscr{D}_T}(Y,T)_{i,j+1/2}. & \text{(b)} \end{cases} \tag{58}$$

The discrete quantities $\zeta(T)^{i,j}_{i+1/2,j}$ and $\zeta(T)^{i,j}_{i,j+1/2}$ are the *entropic corrections* introduced in the discrete diffusion operator $\widehat{\mathscr{D}}_T(Y,T)_{i,j}$ in the cell (i,j), and converge to 1 when Δx and Δy converge to zero (i.e. when $T_{i+1,j} \to T_{i,j}$ and $T_{i,j+1} \to T_{i,j}$). They will be defined in Lemma 3.2 with (67) (or more explicitly with (69)). The necessity to correct the discrete diffusion operator $\mathscr{D}_T(Y,T)$ in the temperature equation (38)(b) with the corrective terms $\zeta(T)^{i,j}_{i+1/2,j}$ and $\zeta(T)^{i,j}_{i,j+1/2}$ will clearly appear in Corollary 3.1. Let us underline that these correction terms could make *non-conservative* the discrete operator $\widehat{\mathscr{D}}_T(Y,T)_{i,j}$ since $\zeta(T)^{i,j}_{i+1/2,j}$ and $\zeta(T)^{i,j}_{i,j+1/2}$ may, respectively, be different from $\zeta(T)^{i+1,j}_{i+1/2,j}$ and $\zeta(T)^{i,j+1}_{i,j+1/2}$. This last point has not to be a priori seen as a "*strange characteristic*" of the scheme *since the continuous equation (36)(b) is not a conservative equation* (in other words, the quantity $\int_\Omega T\,\mathrm{d}x$ is not conserved; see Lemma 2.4 for the conserved quantities).

Computation of the entropic correction $\zeta(T)$ and entropic properties of the scheme:

The necessity to correct the discrete diffusion operator $\mathscr{D}_T(Y,T)$ in (38)(b) with the corrective terms $\zeta(T)^{i,j}_{i+1/2,j}$ and $\zeta(T)^{i,j}_{i,j+1/2}$ is explained in the case of two perfect gases satisfying $\beta_1 = \beta_2$. In that situation, we have $P'(t) = 0$ – thus, $P(t \geqslant 0) = P(t=0) = P^0 - \alpha(Y,T,P^0) = 1/T$, and $\beta(Y,T,P^0)$, $\Gamma(Y,T,P^0)$ are two strictly positive constants (see Section 4).

We have the following result whose proof is immediate:

Lemma 3.1. *When the two fluids are perfect gases verifying $\beta_1 = \beta_2 := \beta$ where β is a strictly positive constant, the system (36) and (37) with the boundary conditions (8)(b) and (9)(c)(d) is given by*

$$\begin{cases} \partial_t Y + \kappa\lambda(Y,T,P^0)\nabla T\cdot\nabla Y = 0, & (a)\\ \partial_t T + \kappa\lambda(Y,T,P^0)(\nabla T)^2 = \kappa T\nabla\cdot[\lambda(Y,T,P^0)\nabla T], & (b)\\ \nabla T(t,x)\cdot n(x)|_{\partial\Omega} = 0, & (c)\\ T|_{\Sigma_1(t)} = T|_{\Sigma_2(t)}, & (d)\\ \lambda\nabla T|_{\Sigma_1(t)}\cdot n_{1\to 2} = \lambda\nabla T|_{\Sigma_2(t)}\cdot n_{1\to 2} & (e) \end{cases} \tag{59}$$

where $\kappa := \beta/P^0$ is a strictly positive constant. Moreover, the system (59) is equivalent to the system

$$\begin{cases} \partial_t Y + \kappa\lambda(Y,\mu^{-1},P^0)\nabla\mu^{-1}\cdot\nabla Y = 0, & (a)\\ \partial_t \mu = \kappa\nabla\cdot[\lambda(Y,\mu^{-1},P^0)\nabla\log\mu], & (b)\\ \nabla\mu(t,x)\cdot n(x)|_{\partial\Omega} = 0, & (c)\\ \mu|_{\Sigma_1(t)} = \mu|_{\Sigma_2(t)}, & (d)\\ \lambda\nabla\mu|_{\Sigma_1(t)}\cdot n_{1\to 2} = \lambda\nabla\mu|_{\Sigma_2(t)}\cdot n_{1\to 2} & (e) \end{cases} \tag{60}$$

with

$$\mu = \frac{1}{T}. \tag{61}$$

Eq. (59)(b) is a Hamilton–Jacobi equation with a *non-conservative* diffusion term. The system (60) can be written in 1D with

$$\begin{cases} \partial_t\mu = \kappa\partial_x[\widehat{\lambda}_1(\mu)\partial_x\mu] \text{ if } x < \Sigma(t),\\ \partial_t\mu = \kappa\partial_x[\widehat{\lambda}_2(\mu)\partial_x\mu] \text{ if } x > \Sigma(t),\\ \widehat{\lambda}_k(\mu) = \lambda_k(\mu^{-1},P^0)/\mu \end{cases} \tag{62}$$

with the conditions at the moving interface $x = \Sigma(t)$

$$\begin{cases} \dfrac{\mathrm{d}}{\mathrm{d}t}\Sigma(t) = -K(\mu)\cdot q(t) \text{ with } K(\mu) := \kappa/\mu,\\ \mu|_{\Sigma^-(t)} = \mu|_{\Sigma^+(t)},\\ \widehat{\lambda}_1(\mu)\partial_x\mu|_{\Sigma^-(t)} = \widehat{\lambda}_2(\mu)\partial_x\mu|_{\Sigma^+(t)} := q(t). \end{cases} \tag{63}$$

Thus, the system (60) is also a *Stefan problem*. This kind of Stefan problem is for example studied in [46] to model phase change phenomena. In [16], we explicit auto-similar solutions of (62) and (63).

The advantage of Eq. (60)(b) is that it is a *conservative* equation oppositely to Eq. (59)(b), and that we immediately obtain that $\mathscr{S}(\mu)(t) := \int_\Omega \mu\log\mu\,\mathrm{d}x$ is a decreasing function whose infimum is equal to $\mathscr{S}(\mu^\infty)$ with $\mu^\infty(x) = C^{st} = \int_\Omega \mu(t=0,x)\,\mathrm{d}x/\int_\Omega \mathrm{d}x$. Thus, using the equivalence Lemma 3.1, we find that the quantity $\mathscr{S}(T)(t) := -\int_\Omega \frac{\log T}{T}\mathrm{d}x$ is also a decreasing function for the system (59) whose infimum is equal to $\mathscr{S}(T^\infty)$ with $T^\infty(x) = C^{st}$. Let us note that the quantity $\mathscr{S}(T)(t)$ is the thermodynamic entropy (up to a multiplicative positive constant) when the two fluids are perfect gases verifying $\beta_1 = \beta_2$ (see also Sections 4.2 and 4.3). In other words, we recover the conclusion of Lemma 2.2 in a particular case.

The idea is now to take advantage of the equivalence between the systems (59) and (60) to obtain an entropic scheme at the semi-discrete level. More precisely, since it is not difficult to obtain a semi-discrete entropic scheme for the system (60) – which is not a priori the case for the system (59) –, we will define the discrete

diffusion operator $\widehat{\mathscr{D}}_T(Y,T)$ used in the scheme (38)(b) in such a way Lemma 3.1 is also verified at the *semi-discrete level*. Let us underline that this approach was also applied with success in the field of kinetic equations to obtain a H-theorem at the semi-discrete level and to obtain an entropic scheme at the fully discretized level [6,12].

The equivalence of the systems (59) and (60) at the *semi-discrete level* is obtained in the following lemma:

Lemma 3.2. *Let us suppose that the two fluids are perfect gases verifying* $\beta_1 = \beta_2 := \beta$ *where* β *is a strictly positive constant and let us define the discrete diffusion operator* $\mathscr{D}_\mu(Y,\mu)$ *with* (51) *and with*

$$\begin{cases} \mathscr{F}^x_{\mathscr{D}_\mu}(Y,\mu)_{i+1/2,j} = \dfrac{\lambda_{i+1/2,j}}{\mu_{i+1/2,j}} \cdot \dfrac{\mu_{i+1,j}-\mu_{i,j}}{\Delta x}, & (a) \\ \mathscr{F}^y_{\mathscr{D}_\mu}(Y,\mu)_{i,j+1/2} = \dfrac{\lambda_{i,j+1/2}}{\mu_{i,j+1/2}} \cdot \dfrac{\mu_{i,j+1}-\mu_{i,j}}{\Delta y} & (b) \end{cases} \tag{64}$$

where $\mu_{i+1/2,j}$ *is a symmetric average of* $\mu_{i,j}$ *and* $\mu_{i+1,j}$*, and where* $\mu_{i,j+1/2}$ *is a symmetric average of* $\mu_{i,j}$ *and* $\mu_{i,j+1}$*. With these definitions, the semi-discrete equation*

$$\partial_t T_{i,j} + \mathscr{T}_T(\Phi,T)_{i,j} = \kappa T_{i,j} \widehat{\mathscr{D}}_T(Y,T)_{i,j} \tag{65}$$

where $\mathscr{T}_T(\Phi,T)$ *and* $\widehat{\mathscr{D}}_T(Y,T)$ *are given by* (55)–(58) *and where* $\kappa := \beta/P^0$ *is equivalent to the semi-discrete equation*

$$\partial_t \mu_{i,j} = \kappa \mathscr{D}_\mu(Y,\mu)_{i,j} \tag{66}$$

with $\mu_{i,j} = 1/T_{i,j}$ *if and only if the corrective term* $\zeta(T)$ *in* (58) *is defined with*

$$\begin{cases} \zeta(T)^{i,j}_{i+1/2,j} = \dfrac{T_{i+1,j}-T_{i,j}}{2T_{i,j}} + \dfrac{1}{\mu_{i+1/2,j}T_{i+1,j}}, & (a) \\ \zeta(T)^{i,j}_{i,j+1/2} = \dfrac{T_{i,j+1}-T_{i,j}}{2T_{i,j}} + \dfrac{1}{\mu_{i,j+1/2}T_{i,j+1}}. & (b) \end{cases} \tag{67}$$

The corrective term $\zeta(T)$ *defines the entropic correction of the discrete operator* $\widehat{\mathscr{D}}_T(Y,T)$.

In (64) and (67), the averages $\mu_{i+1/2,j}$ and $\mu_{i,j+1/2}$ may be defined for example with the symmetric averages (53) or (54) (by replacing λ with μ).

Lemma 3.2 allows to obtain the important corollary:

Corollary 3.1. *The semi-discrete scheme* (65) *verifies*

$$\frac{d}{dt}\mathscr{S}(T)(t) \leqslant 0 \tag{68}$$

with $\mathscr{S}(T) = -\sum_{i,j} \frac{\log T_{i,j}}{T_{i,j}} \Delta x \Delta y$ *when the corrective term* $\zeta(T)$ *is defined with* (67)*. Moreover, when* $\zeta(T) = 1$ *– which is equivalent to* $\widehat{\mathscr{D}}_T(Y,T) = \mathscr{D}_T(Y,T)$ *–, the scheme* (66) *is a non-conservative scheme* although (60)(b) *is a conservative equation.*

The entropy $\mathscr{S}(T) = -\sum_{i,j} \frac{\log T_{i,j}}{T_{i,j}} \Delta x \Delta y$ is the *discrete* thermodynamic entropy when the two fluids are perfect gases verifying $\beta_1 = \beta_2$. The second point of this corollary underlines that it is impossible to prove that the semi-discrete scheme is always entropic when we dot not use the entropic correction that is to say when $\widehat{\mathscr{D}}_T(Y,T) = \mathscr{D}_T(Y,T)$. Numerical results in Section 4.4 confirm this corollary when the time is also discretized by showing that for the proposed test cases, the numerical scheme does not converge when $\widehat{\mathscr{D}}_T(Y,T) = \mathscr{D}_T(Y,T)$ and converges when we use the entropic correction. Let us note that we deduce from formula (67)(a) the two simple formulas

$$\begin{cases} \mu_{i+1/2,j} = \dfrac{2\mu_{i+1,j}\mu_{i,j}}{\mu_{i+1,j}+\mu_{i,j}} \iff \zeta(T)^{i,j}_{i+1/2,j} = \dfrac{T^2_{i+1,j}+T^2_{i,j}}{2T_{i+1,j}T_{i,j}}, & \text{(a)} \\ \mu_{i+1/2,j} = \dfrac{\mu_{i+1,j}+\mu_{i,j}}{2} \iff \zeta(T)^{i,j}_{i+1/2,j} = \dfrac{T^2_{i+1,j}+3T^2_{i,j}}{2T_{i,j}(T_{i+1,j}+T_{i,j})}. & \text{(b)} \end{cases} \tag{69}$$

We have of course similar formulas for $\zeta(T)^{i,j}_{i,j+1/2}$ by using the formula (67)(b). We verify that for the test cases proposed in Section 4, the formulas (69)(a) and (b) give similar results.

Proof of Lemma 3.2. Let us study the $(i+1/2,j)$ term in the scheme (65). We have

$$-\frac{1}{2}u_{i+1/2,j}\cdot\frac{T_{i+1,j}-T_{i,j}}{\Delta x}+\kappa T_{i,j}\frac{\widehat{\mathscr{F}}^{x}_{\mathscr{D}_T}(Y,T)^{i,j}_{i+1/2,j}}{\Delta x}=-\frac{1}{2}u_{i+1/2,j}\cdot\frac{T_{i+1,j}-T_{i,j}}{\Delta x}+\kappa T_{i,j}\zeta(T)^{i,j}_{i+1/2,j}\cdot\frac{\mathscr{F}^{x}_{\mathscr{D}_T}(Y,T)_{i+1/2,j}}{\Delta x}.$$

Moreover, since $\beta^n_{i,j}=\beta$ by hypothesis, the formula (42) shows that

$$\mathscr{P}'(Y^n,T^n,P^n)=\beta\cdot\frac{\sum_{i,j}\mathscr{D}_T(Y^n,T^n)_{i,j}\Delta x\Delta y}{\sum_{i,j}\frac{\Delta x\Delta y}{T^n_{i,j}}}=0$$

since $\mathscr{D}_T(Y,T)$ is a conservative operator and because of the boundary condition (8)(b) on $\partial\Omega$. Thus, Eq. (39) takes the form

$$\Delta_{\Delta x,\Delta y}(\Phi^n)=\kappa\mathscr{D}_T(Y^n,T^n)$$

which implies that $\frac{\Phi_{i+1,j}-\Phi_{i,j}}{\Delta x}=\kappa\lambda_{i+1/2,j}\frac{T_{i+1,j}-T_{i,j}}{\Delta x}$. Using (44), we deduce that

$$u_{i+1/2,j}=\kappa\lambda_{i+1/2,j}\frac{T_{i+1,j}-T_{i,j}}{\Delta x}.$$

Thus

$$\begin{aligned}&-\frac{1}{2}u_{i+1/2,j}\cdot\frac{T_{i+1,j}-T_{i,j}}{\Delta x}+\kappa T_{i,j}\frac{\widehat{\mathscr{F}}^{x}_{\mathscr{D}_T}(Y,T)^{i,j}_{i+1/2,j}}{\Delta x}\\&=\kappa\frac{\lambda_{i+1/2,j}}{\Delta x^2}(T_{i+1,j}-T_{i,j})\left[-\frac{1}{2}(T_{i+1,j}-T_{i,j})+T_{i,j}\zeta(T)^{i,j}_{i+1/2,j}\right]\\&=\kappa\frac{\lambda_{i+1/2,j}}{\Delta x^2}\cdot\frac{T_{i+1,j}-T_{i,j}}{\mu_{i+1/2,j}}\cdot\frac{T_{i,j}}{T_{i+1,j}}=-\kappa\frac{\lambda_{i+1/2,j}}{\Delta x^2}\cdot\frac{\mu_{i+1,j}-\mu_{i,j}}{\mu_{i+1/2,j}}\cdot\frac{1}{\mu^2_{i,j}}=-\frac{\kappa}{\mu^2_{i,j}}\cdot\frac{\mathscr{F}^{x}_{\mathscr{D}_\mu}(Y,T)_{i+1/2,j}}{\Delta x}\end{aligned}$$

by using (64)(a) and (67)(a). By doing same calculus on the other terms, we finally obtain that $-\mathscr{T}_T(\Phi,T)_{i,j}+\kappa T_{i,j}\widehat{\mathscr{D}}_T(Y,T)_{i,j}=-\frac{\kappa}{\mu^2_{i,j}}\mathscr{D}_\mu(Y,\mu)_{i,j}$ that is to say

$$\partial_t T_{i,j}=-\frac{\kappa}{\mu^2_{i,j}}\mathscr{D}_\mu(Y,\mu)_{i,j}.$$

We conclude by noting that $\partial_t T_{i,j}=-\mu^{-2}_{i,j}\partial_t\mu_{i,j}$. □

Proof of Corollary 3.1. For sake of simplicity, we write the proof in the 1D case, the proof in the 2D (and 3D) case being the same. We have

$$\mathscr{S}(T)(t):=-\sum_i\frac{\log T_i}{T_i}\Delta x=\sum_i\mu_i\log\mu_i\Delta x.$$

Thus, the time-derivative of $\mathscr{S}(T)(t)$ is equal to

$$\frac{d}{dt}\mathscr{S}(T)(t)=\sum_i\partial_t\mu_i\Delta x+\sum_i\log\mu_i\partial_t\mu_i\Delta x.$$

And since the semi-discrete scheme (65) is equivalent to the semi-discrete scheme (66) (cf. Lemma 3.2), we obtain that $\sum_i\partial_t\mu_i\Delta x=\kappa\sum_i\mathscr{D}_\mu(Y,\mu)_i\Delta x=0$ (since $\mathscr{D}_\mu(Y,\mu)$ is a conservative operator) and $\sum_i\log\mu_i\partial_t\mu_i\Delta x=\kappa\sum_i\log\mu_i\mathscr{D}_\mu(Y,\mu)_i\Delta x$. This implies that

$$\begin{aligned}\frac{d}{dt}\mathscr{S}(T)(t)&=\kappa\sum_i\log\mu_i\mathscr{D}_\mu(Y,\mu)_i\Delta x=\kappa\sum_i\log\mu_i[\mathscr{F}^{x}_{\mathscr{D}_\mu}(Y,\mu)_{i+1/2}-\mathscr{F}^{x}_{\mathscr{D}_\mu}(Y,\mu)_{i-1/2}]\\&=\kappa\sum_i(\log\mu_i-\log\mu_{i+1})\mathscr{F}^{x}_{\mathscr{D}_\mu}(Y,\mu)_{i+1/2}=-\kappa\sum_i(\log\mu_{i+1}-\log\mu_i)(\mu_{i+1}-\mu_i)\frac{\lambda_{i+1/2}}{\mu_{i+1/2}\Delta x}.\end{aligned}$$

We obtain that $\frac{d}{dt}\mathscr{S}(T)(t) \leqslant 0$ by noting that $\kappa > 0$ and that $(\log \mu_{i+1} - \log \mu_i)(\mu_{i+1} - \mu_i) \geqslant 0$ since $x \mapsto \log x$ is an increasing function. Let us underline that this result is obtained for any $\mu_{i+1/2} > 0$ and, thus, for any corrective term $\zeta(T)^i_{i+1/2}$ verifying the formula (67)(a). To prove the second point, we just have to note that $\zeta(T)^i_{i+1/2} = 1$ is equivalent to $\mu_{i+1/2} = \frac{2\mu^2_{i+1}}{3\mu_{i+1}-\mu_i}$ which is a non-symmetric formula. □

3.4. Interface capturing algorithm: the operator $\mathscr{T}_Y(\Phi, Y)$

We now define the discrete operator $\mathscr{T}_Y(\Phi, Y)$ used in (38)(a) to discretize the 2D transport equation (36)(a). Firstly, we recall the splitting technique which allows to uncouple the directions x and y. Secondly, we recall the 1D *non-diffusive* scheme proposed by Després and Lagoutière in [18,19,31] and we describe the extension in our context of this 1D scheme. This extension will be used to define the operator $\mathscr{T}_Y(\Phi, Y)$. Because of the properties of the Després–Lagoutière's non-diffusive scheme, we obtain a first order operator $\mathscr{T}_Y(\Phi, Y)$ which defines a 2D scheme (38)(a) diffusing any initial Heaviside function Y^0 on a small number of cells (between one and three) during the transient regime.

3.4.1. Splitting of the 2D transport equation (36)(a)

To solve the transport equation (36)(a) in 2D, we split the directions x and y. This means that we successively solve the two transport equations

$$\partial_t Y + v(t,x,y)\partial_x Y = 0 \text{ with } v(t,x,y) := \partial_x \Phi$$

and

$$\partial_t Y + v(t,x,y)\partial_y Y = 0 \text{ with } v(t,x,y) := \partial_y \Phi$$

at each time step. Thus, we discretize (36)(a) with the scheme

$$\begin{cases} Y^*_{i,j} = Y^n_{i,j} - \Delta t \cdot \mathscr{T}^x_Y(\Phi^n, Y^n)_{i,j}, & \text{(a)} \\ Y^{n+1}_{i,j} = Y^*_{i,j} - \Delta t \cdot \mathscr{T}^y_Y(\Phi^n, Y^*)_{i,j} & \text{(b)} \end{cases} \tag{70}$$

where $\mathscr{T}^x_Y(\Phi, Y)$ and $\mathscr{T}^y_Y(\Phi, Y)$ discretize, respectively, the continuous operators $\partial_x \Phi \partial_x Y$ and $\partial_y \Phi \partial_y Y$. In other words, the operator $\mathscr{T}_Y(\Phi, Y)$ is defined with the formula

$$\mathscr{T}_Y(\Phi, Y) = \mathscr{T}^x_Y(\Phi^n, Y^n)_{i,j} + \mathscr{T}^y_Y(\Phi^n, Y^*)_{i,j} \text{ where } Y^*_{i,j} = Y^n_{i,j} - \Delta t \cdot \mathscr{T}^x_Y(\Phi^n, Y^n)_{i,j}. \tag{71}$$

Let us underline that we can use this splitting technique because the 2D mesh is cartesian. The importance of this splitting approach will be underlined in Section 3.4.4.

It remains to define the discrete operators $\mathscr{T}^x_Y(\Phi, Y)$ and $\mathscr{T}^y_Y(\Phi, Y)$ used in (71). Since the previous splitting approach is equivalent to solve successively two 1D transport equations, we just have to define the operator $\mathscr{T}^x_Y(\Phi, Y)$ in the 1D case

$$\partial_t Y + v(t,x)\partial_x Y = 0 \text{ where } v(t,x) := \partial_x \Phi \text{ is a given function.} \tag{72}$$

The extension for $\mathscr{T}^x_Y(\Phi, Y)$ and $\mathscr{T}^y_Y(\Phi, Y)$ in the 2D case will be immediate. To define the operator $\mathscr{T}^x_Y(\Phi, Y)$ in the 1D case, we extend to the case $v(t,x) \neq C^{st}$ the *non-diffusive* scheme proposed in [18,19,31] for the resolution of the 1D transport equation $\partial_t Y + v\partial_x Y = 0$ where $v = C^{st}$. We recall in Section 3.4.2 this non-diffusive scheme and its basic properties (see Lemma 3.3) and we explicit this extension in Section 3.4.3.

3.4.2. Discretization of $\partial_t Y + v\partial_x Y = 0$ with $v := C^{st}$ with a non-diffusive scheme

The Després–Lagoutière's non-diffusive scheme was proposed and studied in [18]. This scheme enters in the class of schemes using the slope-limiters formalism [43] and is equivalent to the ultrabee scheme [44]. This scheme has been rewritten with an equivalent formulation in [19] (see also [31]) which does not use explicitly the slope-limiters formalism. This formulation is given by

$$Y_i^{n+1} = Y_i^n - \frac{\Delta t}{\Delta x} v \cdot [\mathscr{Y}_{i+1/2}^n(v) - \mathscr{Y}_{i-1/2}^n(v)] \tag{73}$$

where

$$\mathscr{Y}_{i+1/2}(v) = \begin{cases} b_i(v) & \text{if } Y_{i+1} \leqslant b_i(v), \\ Y_{i+1} & \text{if } b_i(v) < Y_{i+1} < B_i(v), \\ B_i(v) & \text{if } B_i(v) \leqslant Y_{i+1} \end{cases} \tag{74}$$

with

$$\begin{cases} b_i(v) := \dfrac{Y_i - \max(Y_{i-1}, Y_i)}{v\Delta t/\Delta x} + \max(Y_{i-1}, Y_i), \\ B_i(v) := \dfrac{Y_i - \min(Y_{i-1}, Y_i)}{v\Delta t/\Delta x} + \min(Y_{i-1}, Y_i). \end{cases} \tag{75}$$

Of course, when $v = C^{st} < 0$, we have to change (74) and (75) with symmetric formulas. This scheme is interesting because of the following lemma [18,19,31]:

Lemma 3.3. *Under the CFL criteria $\Delta t < \Delta x/v$, the scheme (73)–(75) is convergent, is such that $0 \leqslant Y_i^n \leqslant 1 \Rightarrow 0 \leqslant Y_i^{n+1} \leqslant 1$ and diffuses any Heaviside function on only one cell which means that the numerical diffusion is controlled uniformly in time.*

The main advantage of the scheme (73)–(75) is that any 1D interface captured by this scheme remains sharp *for any integration time*. Let us note that it is easy to prove that when the initial condition is a Heaviside function, the 1D scheme (73)–(75) is equivalent to the *reservoir scheme* proposed in [3]. The advantage of the formulation (73)–(75) is that it enters into the field of finite-volume schemes (which allows to obtain convergence results with classical techniques) and that the 2D (or 3D) extension is immediate through the splitting technique described in Section 3.4.1. To our knowledge, the extension in 2D and 3D of the *reservoir scheme* formalism is not so natural.

3.4.3. The operator $\mathscr{T}_Y^x(\Phi, Y)$ in the 1D case

We now discretize the 1D transport equation (72) with $v(t,x) \neq C^{st}$ by extending the scheme (73)–(75) to our context. Let us underline that the possibility of this extension is mentioned in [31]. The idea is to suppose that, locally to the cell i, the velocity $v(t,x) \in]x_{i-1/2}, x_{i+1/2}[$ is a constant v_i. Thus, we define the scheme

$$Y_i^{n+1} = Y_i^n - \Delta t \cdot \mathscr{T}_Y^x(\Phi^n, Y^n)_i \tag{76}$$

and the operator $\mathscr{T}_Y^x(\Phi, Y)$ with

$$\mathscr{T}_Y^x(\Phi, Y)_i = \frac{1}{\Delta x} \cdot \frac{\Phi_{i+1} - \Phi_{i-1}}{2\Delta x} \cdot [Y_{i+1/2}^{\text{left}}(\Phi) - Y_{i-1/2}^{\text{right}}(\Phi)] \tag{77}$$

with

$$\begin{cases} Y_{i+1/2}^{\text{left}}(\Phi) = \mathscr{Y}_{i+1/2}\left(\dfrac{\Phi_{i+1} - \Phi_{i-1}}{2\Delta x}\right), \\ Y_{i+1/2}^{\text{right}}(\Phi) = \mathscr{Y}_{i+1/2}\left(\dfrac{\Phi_{i+2} - \Phi_i}{2\Delta x}\right) \end{cases} \tag{78}$$

where $\mathscr{Y}_{i+1/2}(v)$ is given by (74) when $v > 0$ (and by the symmetric formulas when $v < 0$). Let us note that $\frac{\Phi_{i+1} - \Phi_{i-1}}{2\Delta x}$ is an approximation of the potential velocity field in the cell i and that

$$\frac{u_{i+1/2} + u_{i-1/2}}{2} = \frac{\Phi_{i+1} - \Phi_{i-1}}{2\Delta x}$$

where the discrete potential velocity field $u_{i+1/2}$ is given by (44)(a). Of course, the scheme (76)–(78) is consistent with Eq. (72).

The important point of this subsection is the following result:

Lemma 3.4. *Under the CFL criteria* $\Delta t < \Delta x/\max_i|u^n_{i+1/2}|$, *the scheme (76)–(78) is such that* $0 \leqslant Y^n_i \leqslant 1 \Rightarrow 0 \leqslant Y^{n+1}_i \leqslant 1$ *and diffuses any Heaviside function on only one cell which means that the numerical diffusion is controlled uniformly in time.*

The proof of this lemma relies on the fact that, *locally* to any cell i, the scheme (76)–(78) is identical to the scheme (73)–(75) which implies that the conclusions of Lemma 3.3 are still valid.

3.4.4. Remark on the importance of the splitting technique

The use of the Després–Lagoutière's non-diffusive scheme makes necessary to split the directions x and y to define the operator $\mathscr{T}_Y(\Phi, Y)$ in the 2D case. Indeed, the 2D scheme

$$Y^{n+1}_{i,j} = Y^n_{i,j} - \frac{\Delta t}{\Delta x} v_x \cdot [\mathscr{Y}^n_{i+1/2,j}(v_x) - \mathscr{Y}^n_{i-1/2,j}(v_x)] - \frac{\Delta t}{\Delta y} v_y \cdot [\mathscr{Y}^n_{i,j+1/2}(v_y) - \mathscr{Y}^n_{i,j-1/2}(v_y)]$$

used to discretize the 2D equation $\partial_t Y + v \cdot \nabla Y = 0$ (with $v = (v_x > 0, v_y > 0) = C^{ste}$) is not stable when $\mathscr{Y}_{i+1/2,j}(v_x)$ and $\mathscr{Y}_{i,j+1/2}(v_y)$ are defined with (74) [31]. Moreover, by applying Lemma 3.4 in each direction, we obtain that the 2D operator $\mathscr{T}_Y(\Phi, Y)$ obtained by using the splitting technique verifies $0 \leqslant Y^n_{i,j} \leqslant 1 \Rightarrow 0 \leqslant Y^{n+1}_{i,j} \leqslant 1$ under the CFL criteria $\Delta t < \min(\Delta x/\max_{i,j}|u^n_{i+1/2,j}|, \Delta y/\max_{i,j}|u^n_{i,j+1/2}|)$. And we numerically verify that for the test cases proposed in Section 4, the 2D Heaviside function is diffused during the transient regime on a limited number of cells (between one and three): this means that the *accuracy* objective of the *two-steps approach* (cf. Section 1) is realized.

4. Numerical results in the case of two perfect gases

We now propose 2D numerical results on the domain Ω equal to the open square $]-1,1[\times]-1,1[$. Let us recall that the mesh is cartesian. In the proposed numerical tests, we have $\Delta x = \Delta y$. Nevertheless, we could also apply our algorithm with $\Delta x \neq \Delta y$.

We firstly show in Section 4.1 that the 2D interface capturing algorithm proposed in Section 3.4 is accurate by applying this algorithm to the numerical resolution of the 2D non-linear hyperbolic-elliptic system introduced in [15]. This system models strong vibrations of a surface $\Sigma(t)$ and the volume $\mathscr{V}(t)$ bounded by $\Sigma(t)$ is also solution of an ordinary differential equation which can be solved explicitly: thus, we can test the robustness and the accuracy of our 2D interface capturing algorithm. Secondly, we propose 2D numerical results for the potential DLMN-$\mathscr{M}$ system when the two fluids are perfect gases, the equations of state and the physical constants being defined in Section 4.2. This case is important for two reasons: firstly, it allows to explicit for any initial conditions the thermodynamic equilibrium defined by $(T^\infty, P^\infty, S_1^\infty)$ and, thus, allows to study the accuracy of the algorithm, the quantity S_1^∞ being the surface of the bubbles of fluid 1 when $(T, P) = (T^\infty, P^\infty)$: see Section 4.3; secondly, it is necessary to validate the way we used to define the *entropic correction* in Section 3.3 before simulating the DLMN system with more complicated equations of state.

The first test case proposed in Section 4.4 validates the convergence of the scheme toward a good thermodynamic equilibrium and confirms the importance of the *entropic correction*, at least when the initial temperature differences are large. To define this correction, we use the formula (69)(a) (the formula (69)(b) gives similar results for the proposed test cases). The second test case proposed in Section 4.5 shows that the 2D interface capturing algorithm defined in Section 3.4 allows to capture fine details of the compression and dilation of bubbles, *even when the topological changes are important*. We show in Section 4.6 that the thickness of the artificial mixture area is almost constant and lower than three cells during the transient regime. That property is an important characteristic of our algorithm and is of course directly linked to the properties of the 2D interface capturing algorithm based on the Després–Lagoutière's non-diffusive scheme [18,19,31] (see Lemmas 3.3 and 3.4). At last, we numerically show in Section 4.7 that the scheme converges with a first order error and we study the value of the time step Δt during the transient regime.

The time step Δt is such that

$$\Delta t = \mathrm{CFL} \times \min(\Delta t_u, \Delta t_T) \tag{79}$$

with $\mathrm{CFL} = 1/5$ where

$$\begin{cases} \Delta t_u = \dfrac{\Delta x}{\max\limits_{i,j}(|u_{i+1/2,j}|, |u_{i,j+1/2}|)}, & \text{(a)} \\ \Delta t_T = \dfrac{P^n}{\max\limits_{i,j}(\beta^n_{i,j}\lambda^n_{i,j}/\alpha^n_{i,j})} \min(\Delta x^2, \Delta y^2). & \text{(b)} \end{cases} \tag{80}$$

We numerically verify that the constraint (79) is sufficient to obtain the stability of our algorithm. Let us note that we could relax the constraint (79) by taking CFL $> 1/5$ (indeed, CFL $\in [0,2/5]$ seems to define a stability limit area for our explicit algorithm). The constraint $\Delta t \leqslant \Delta t_u$ is imposed by the explicit 2D interface capturing algorithm (38)(a); the constraint $\Delta t \leqslant \Delta t_T$ is imposed by the diffusive part of the explicit scheme (38)(b).

The thermodynamic pressure P^{n+1} is computed with the operator $\mathscr{P}$ defined with the implicit scheme (45)(c). This operator makes conservative the scheme in total mass (let us recall that with this choice, the scheme cannot conserve the mass of the fluid 1 and the energy of the system). The operator $\mathscr{P}$ given by (45)(c) is implicit. Nevertheless, when the two fluids are perfect gases, the operator $\mathscr{P}$ is explicit. Indeed, we easily obtain that (45)(c) coupled to the closure law (28)(a) and to the equation of state (84)(a) gives

$$P^{n+1} = \mathscr{P}(Y^n, Y^{n+1}, T^n, T^{n+1}, P^n) := P^n \cdot \frac{\sum_{i,j} \dfrac{\Delta x \Delta y}{R^n_{i,j} T^n_{i,j}}}{\sum_{i,j} \dfrac{\Delta x \Delta y}{R^{n+1}_{i,j} T^{n+1}_{i,j}}}$$

with $R^n_{i,j} := Y^n_{i,j} R_1 + (1 - Y^n_{i,j}) R_2$. Let us note that for the two test cases proposed in this section, the numerical results are equivalent when the operator $\mathscr{P}$ is defined with (45)(a) or (b), or with (48) or (49). At last, the initial pressure $P^0 = P(t = 0)$ is equal to 10^3. This high pressure implies that the initial Mach number is lower than 3×10^{-2} in the two test cases. Since the Mach number decreases exponentially to zero, the low Mach number condition – which defined the physical validity domain of the DLMN system – is always satisfied. This exponential decreasing also underlines that it would be necessary to use good preconditioning techniques and robust iterative solvers to reproduce these two test cases with implicit diphasic compressible Navier–Stokes solvers.

4.1. Preliminary results: discretization of an abstract bubbles vibration model

In [15], we have established an existence and uniqueness result for a classical solution of the non-linear hyperbolic-elliptic system

$$\begin{cases} \partial_t Y + \nabla \Phi \cdot \nabla Y = 0, & \text{(a)} \\ Y(t = 0, x) = Y^0(x), & \text{(b)} \\ \Delta \Phi = \psi(t) \cdot \mathscr{P}(Y), & \text{(c)} \\ \nabla \Phi \cdot n|_{\partial\Omega} = 0 & \text{(d)} \end{cases} \tag{81}$$

defined on $[0, +\infty[\times \Omega$, the function $\mathscr{P}(Y)$ being given by $\mathscr{P}(Y) = Y - \frac{\int_\Omega Y \, dx}{\int_\Omega dx}$. The function $\psi(t) \in \mathscr{C}([0, +\infty[)$ is a given function which imposes the frequency of the vibrations of $\Sigma(t)$ when the initial condition is given by (7). Let us remark that the system (81) and the potential DLMN-$\mathscr{M}$ system have a similar mathematical structure. An important property of the system (81) is given in the following lemma [15]:

Lemma 4.1. *When the initial condition $Y(t = 0,x)$ is given by (7), the volume $\mathscr{V}(\Omega_1(t)) := \int_{\Omega_1(t)} dx$ of the bubble $\Omega_1(t)$ is solution of the ordinary differential equation*

$$\begin{cases} f'(t) = \psi(t) \cdot f(t)[1 - f(t)], \\ f(t = 0) = \dfrac{\mathscr{V}(\Omega_1(t = 0))}{\mathscr{V}(\Omega)} \end{cases}$$

with $f(t) := \frac{\mathscr{V}(\Omega_1(t))}{\mathscr{V}(\Omega)}$ *and* $\mathscr{V}(\Omega) := \int_\Omega dx$. *Thus, the volume of the bubble* $\Omega_1(t)$ *is given by*

$$\mathscr{V}(\Omega_1(t)) = \mathscr{V}(\Omega) \cdot \frac{\mathscr{V}(\Omega_1(t=0)) \exp(\int_0^t \psi(\tau)\, d\tau)}{\mathscr{V}(\Omega_2(t=0)) + \mathscr{V}(\Omega_1(t=0)) \exp(\int_0^t \psi(\tau)\, d\tau)}, \tag{82}$$

where $\mathscr{V}(\Omega_2(t=0)) := \mathscr{V}(\Omega) - \mathscr{V}(\Omega_1(t=0))$.

This lemma allows to study *carefully* the accuracy of the 2D interface capturing algorithm proposed in Section 3.4 by comparing the quantity

$$\mathscr{V}_{\Delta x,\Delta y}(\Omega_1(t^n)) = \sum_{i,j} Y_{i,j}^n \Delta x \Delta y \tag{83}$$

to the quantity $\mathscr{V}(\Omega_1(t^n))$ deduced from the formula (82). Thus, we solve the system (81) in 2D geometry by using the numerical schemes (38)(a) and (39) with now

$$G^n = \psi(t^n) \cdot \left[Y_{i,j}^n - \frac{\sum_{k,l} Y_{k,l}^n \Delta x \Delta y}{(y_{\max} - y_{\min})(x_{\max} - x_{\min})} \right].$$

To impose *strong* non-periodic vibrations to the bubble $\Omega_1(t)$ and, thus, to the interface $\Sigma(t)$, we define $\psi(t)$ with

$$\psi(t) = 3 \times \cos\left(\frac{2\pi t}{\mathscr{T}}\right) \times \cos\left(\frac{2\pi t}{\sqrt{2}\mathscr{T}}\right) \times \cos\left(\frac{2\pi t}{\sqrt{7}\mathscr{T}}\right) \text{ with } \mathscr{T} = 1.$$

To study the accuracy of the algorithm *locally* to the interface $\Sigma(t)$, we define the initial conditions (7) in such a way the bubble $\Omega_1(t=0)$ has the shape of a star and, thus, has a fine structure. Indeed, the system (81) is not a dissipative system and the structure of the interface $\Sigma(t>0)$ should be similar to the structure of $\Sigma(t=0)$ despite the strong vibrations (let us note that the DLMN system is dissipative because of the heat conduction). The time step is defined with $\Delta t = \min(\mathrm{CFL} \times \Delta t_u, \Delta t_\psi)$ with $\mathrm{CFL} = 1/2$ where Δt_u is given by (80)(a) and where $\Delta t_\psi = \frac{\mathscr{T}}{100}$. The time step Δt_ψ is linked to the signal $\psi(t)$ whose high frequency is equal to $2\pi/\mathscr{T}$. We use a 100×100 mesh. Figs. 1–3 show $Y(t,x)$, respectively, when $t^n = 0$ (initial condition), $t^n = 4$ and $t^n = 10$ (which corresponds to $n \simeq 1000$ since $\Delta t_u > 0.019$ and $\Delta t_\psi = 0.01$). Fig. 4 shows the volume $\mathscr{V}(\Omega_1(t))$ of the bubble ($t \in [0,10]$) when it is computed with the analytic formula (82) and with the numerical formula (83) (dashed line). These figures show that the 2D interface capturing algorithm based on the Després–Lagoutière's non-diffusive scheme [18,19,31] is accurate and preserves the fine structure of the interface $\Sigma(t)$, even under strong vibrations.

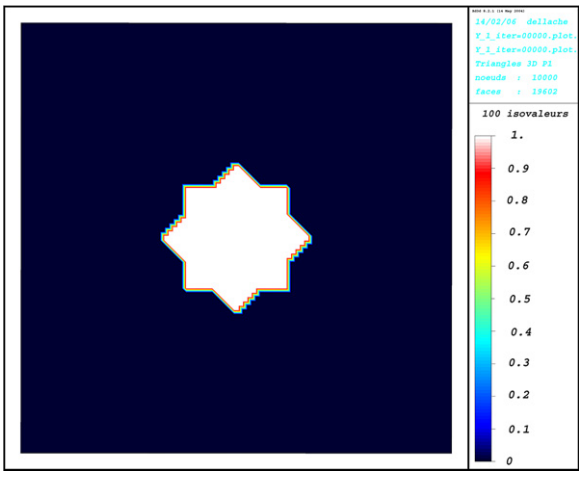

Fig. 1. Initial mass fraction $Y_{i,j}^0$ (abstract model).

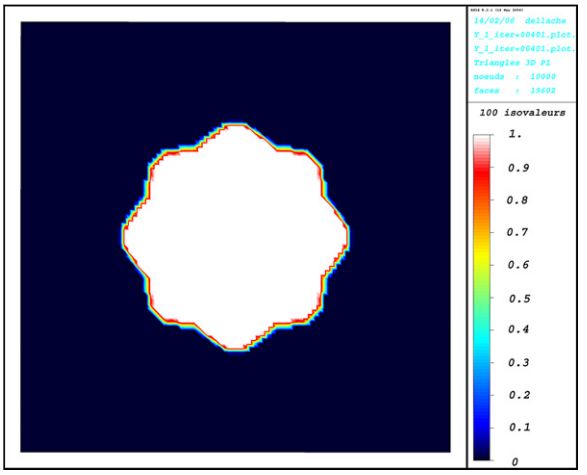

Fig. 2. Mass fraction $Y_{i,j}^n$ when $t^n = 4$ (abstract model).

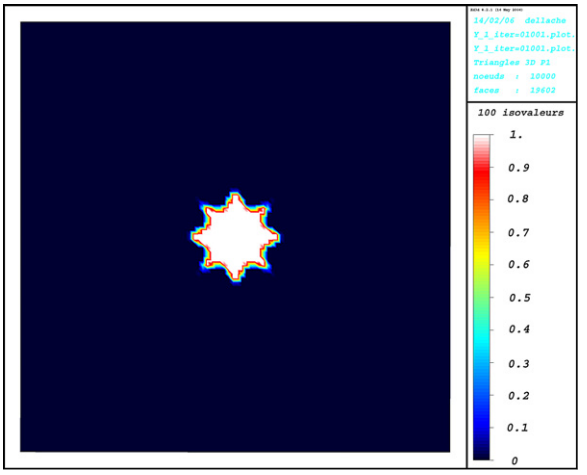

Fig. 3. Mass fraction $Y_{i,j}^n$ when $t^n = 10$ (abstract model).

4.2. Equations of state and physical constants

We now come back to the DLMN system. In this section, we suppose that the two fluids are perfect gases. This means that the equations of state are given by

$$\begin{cases} \rho_k(T,P) = \dfrac{P}{R_k T}, & \text{(a)} \\ \varepsilon_k(T,P) = \varepsilon_k(T) = \dfrac{R_k T}{\gamma_k - 1}, & \text{(b)} \end{cases} \tag{84}$$

where $R_k > 0$, $\gamma_k > 1$ and $k \in \{1,2\}$. In that case, we deduce from (12) and (13) that

$$\begin{cases} \alpha_k(T,P) = \alpha(T) = \dfrac{1}{T}, \\ \beta_k(T,P) = \beta_k = \dfrac{\gamma_k - 1}{\gamma_k}, \\ \Gamma_k(T,P) = \Gamma_k = \gamma_k. \end{cases}$$

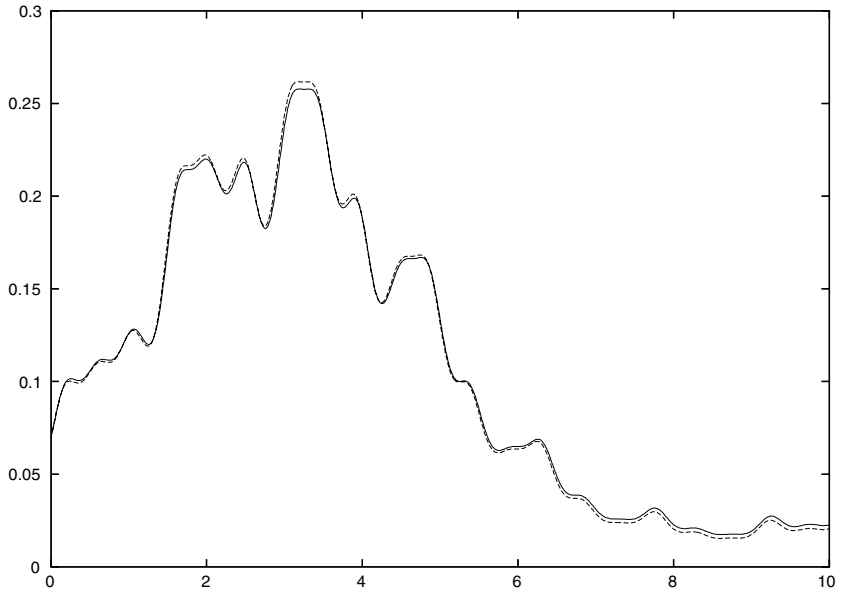

Fig. 4. Volume of the bubble given by (82) and (83) (dashed line) (abstract model).

Moreover, by using (26)–(28), we obtain

$$\rho(Y,T,P) = \frac{P}{\mathscr{R}(Y)T}$$

and

$$\begin{cases} \alpha(Y,T,P) = \alpha(T) = \dfrac{1}{T}, \\ \beta(Y,T,P) = \beta(Y) = \dfrac{\mathscr{R}(Y)}{\mathscr{C}_p(Y)}, \\ \Gamma(Y,T,P) = \Gamma(Y) = \dfrac{1}{1-\beta(Y)}, \end{cases}$$

where $\mathscr{R}(Y) = YR_1 + (1-Y)R_2$ and $\mathscr{C}_p(Y) = Y\frac{R_1\gamma_1}{\gamma_1-1} + (1-Y)\frac{R_2\gamma_2}{\gamma_2-1}$. Let us remark that when $\beta_1 = \beta_2$ that is to say when $\gamma_1 = \gamma_2 := \gamma$, the previous relations show that $\beta(Y,T,P) = (\gamma-1)/\gamma$ and $\Gamma(Y,T,P) = \gamma$: this particular case is used in Lemmas 3.1 and 3.2 to define the *entropic correction*. At last, the conductivity $\lambda_k(T,P)$ is supposed to be a constant λ_k for sake of simplicity (but $\lambda_1 \neq \lambda_2$), and the physical constants are given by

$$\begin{cases} \gamma_1 = 3, \\ R_1 = 1, \\ \lambda_1 = 1 \end{cases} \quad \text{and} \quad \begin{cases} \gamma_2 = 3/2, \\ R_2 = 2, \\ \lambda_2 = 1/2. \end{cases}$$

4.3. Thermodynamic equilibrium of the DLMN system

Lemma 2.1 coupled to the equations of state (84) shows that

$$\begin{cases} \mathscr{M}_k(t) := \dfrac{P(t)}{R_k} \cdot \displaystyle\int_{\Omega_k(t)} \frac{\mathrm{d}x}{T(t,x)} \quad \text{for } k \in \{1,2\}, \\ \mathscr{E}(t) := P(t) \cdot \left(\dfrac{S_1(t)}{\gamma_1 - 1} + \dfrac{S_2(t)}{\gamma_2 - 1} \right) \end{cases} \tag{85}$$

are constants at the continuous level and, thus, are respectively equal to the initial quantities $\mathscr{M}_k(t=0)$ and $\mathscr{E}(t=0)$ knowing that the quantities

$$\begin{cases} S_1(t) = \int_\Omega Y(t,x)\,\mathrm{d}x, \\ S_2(t) = \int_\Omega (1-Y(t,x))\,\mathrm{d}x \end{cases} \tag{86}$$

define the surfaces of $\Omega_1(t)$ and $\Omega_2(t)$ (or the volumes in 3D). Of course, we have also $S_1(t)+S_2(t)=S_\Omega$ where S_Ω is the surface of the domain Ω. By using these relations, we easily obtain that

$$\begin{cases} T^\infty = \mathscr{E}(t=0)\cdot \dfrac{(\gamma_1-1)(\gamma_2-1)}{(\gamma_2-1)R_1\mathscr{M}_1(t=0)+(\gamma_1-1)R_2\mathscr{M}_2(t=0)}, \\ P^\infty = \frac{\mathscr{E}(t=0)}{S_\Omega}\cdot \dfrac{R_1\mathscr{M}_1(t=0)+R_2\mathscr{M}_2(t=0)}{\dfrac{R_1\mathscr{M}_1(t=0)}{\gamma_1-1}+\dfrac{R_1\mathscr{M}_2(t=0)}{\gamma_2-1}}, \\ S_1^\infty = S_\Omega\cdot \dfrac{R_1\mathscr{M}_1(t=0)}{R_1\mathscr{M}_1(t=0)+R_2\mathscr{M}_2(t=0)}. \end{cases} \tag{87}$$

And since the thermodynamic entropy $s_k(T,P)$ is equal to $\frac{P}{\beta_k T}\log(P^{\beta_k}/T)$ when the fluid k is a perfect gas, we deduce the infimum $\mathscr{S}^\infty \equiv \mathscr{S}(Y^\infty,T^\infty,P^\infty)$ of the entropy $\mathscr{S}\equiv\mathscr{S}(Y,T,P)$ – cf. Lemma 2.2 – with the formula

$$\mathscr{S}^\infty = \frac{P^\infty}{T^\infty}\cdot\left[\frac{S_1^\infty}{\beta_1}\log\left(\frac{P^{\infty\beta_1}}{T^\infty}\right)+\frac{S_2^\infty}{\beta_2}\log\left(\frac{P^{\infty\beta_2}}{T^\infty}\right)\right]. \tag{88}$$

The quantity $(T^\infty,P^\infty,S_1^\infty,\mathscr{S}^\infty)$ defines the *continuous* thermodynamic equilibrium of the DLMN system. Of course, we define the *discrete* thermodynamic equilibrium $(T^\infty,P^\infty,S_1^\infty,\mathscr{S}^\infty)$ with (87) and (88) by replacing $\int_\Omega$ with $\sum_{i,j}$ in (85) and (86).

4.4. First test case: dilation of one bubble on a 50×50 mesh

The initial temperature field is given by

$$T^0_{i,j} = 10\times\left[1-\exp\left(-25\frac{x_{i,j}^2+y_{i,j}^2}{2}\right)\right]+10^{-4}.$$

The quantity 10^{-4} is added to impose $T^0_{i,j}>0$ in Ω. We define the initial circular bubble Ω_1^0 with

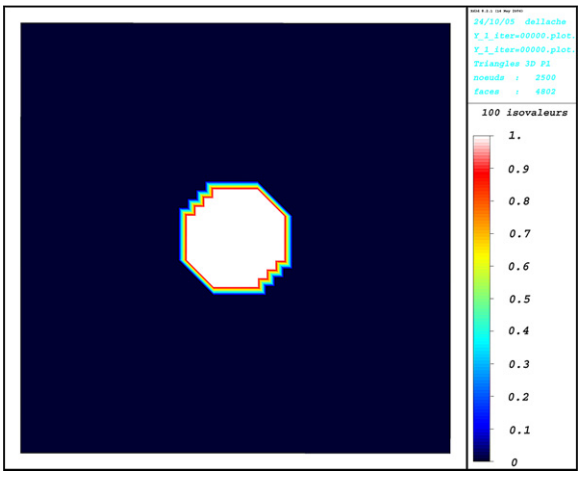

Fig. 5. Initial mass fraction $Y^0_{i,j}$ (first test case).

$$Y^0_{i,j} = \begin{cases} 1 & \text{if } x^2_{i,j} + y^2_{i,j} < (1/4)^2, \\ 0 & \text{if not.} \end{cases}$$

Figs. 5 and 6 show the mass fractions $Y^0_{i,j}$ and $Y^n_{i,j}$ when $t^n = 300$ (which corresponds to $n \simeq 4200$). Fig. 7 shows the pressure $P(t^n)/P^\infty$, the entropy $\mathscr{S}(t^n)/|\mathscr{S}^\infty|$ and the surface $S_1(t^n)/S_1^\infty$ of the bubble $\Omega_1(t^n)$ where the three constants P^∞, $\mathscr{S}^\infty$ and S_1^∞ are given by the discrete thermodynamic equilibrium (87) and (88). Fig. 8 represents $P(t^n)/P^\infty$ and $\mathscr{S}(t^n)/|\mathscr{S}^\infty|$ when we do not use the *entropic correction* introduced in Section 3.3 *i.e.* when $\widehat{\mathscr{D}}_T(Y,T) := \mathscr{D}_T(Y,T)$ in (38)(b). Fig. 9 shows the mass fraction $Y^n_{i,j}$ at $t^n = 300$ when the operator $\mathscr{T}_Y(\Phi, Y)$ is defined with the standard first order upwind scheme. Fig. 10 compares the relative mass error

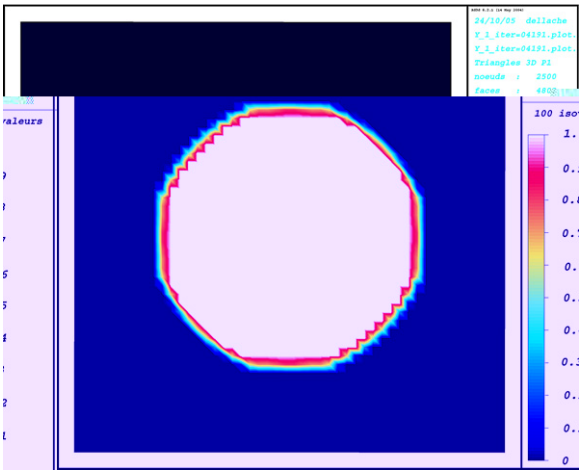

Fig. 6. Mass fraction $Y^n_{i,j}$ when $t^n = 300$ (first test case).

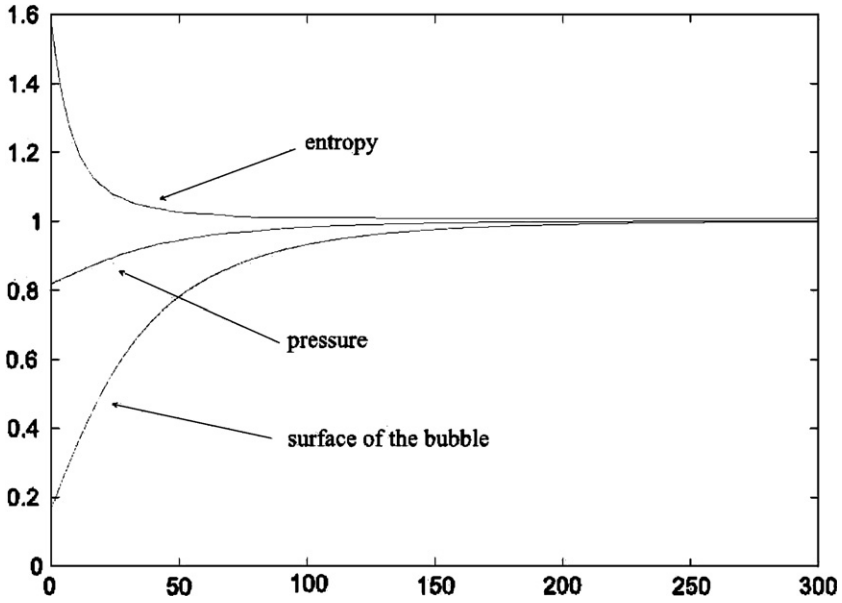

Fig. 7. $P(t)/P^\infty$, $\mathscr{S}(t)/|\mathscr{S}^\infty|$ and $S_1(t)/S_1^\infty$ (first test case).

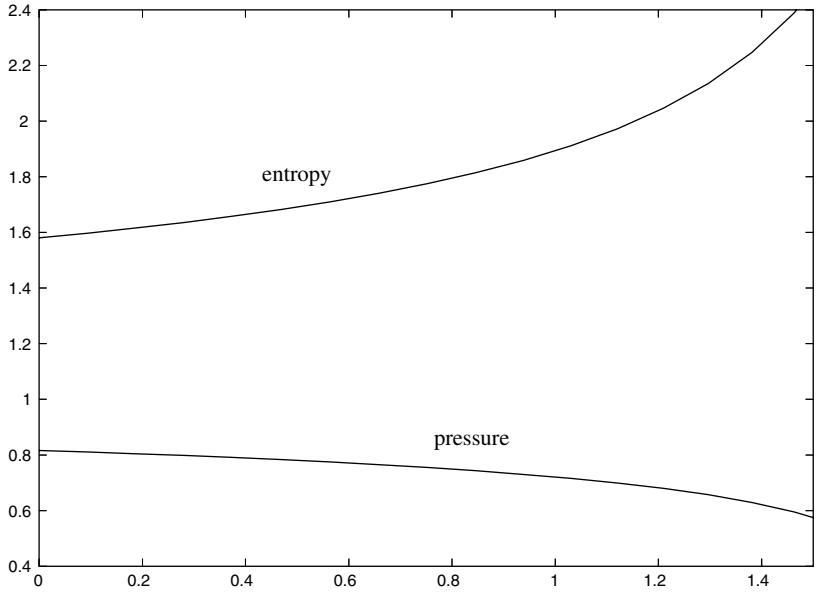

Fig. 8. $P(t)/P^{\infty}$ and $\mathscr{S}(t)/|\mathscr{S}^{\infty}|$ without entropic correction (first test case).

$\epsilon_{M_1}(t^n) = \frac{\sum_{i,j}(Y^n_{i,j}\rho^n_{i,j} - Y^0_{i,j}\rho^0_{i,j})}{\sum_{i,j} Y^0_{i,j}\rho^0_{i,j}}$ of the bubble $\Omega_1(t^n)$ and the relative energy error $\epsilon_E(t^n) = \frac{\sum_{i,j}(\rho^n_{i,j}e^n_{i,j} - \rho^0_{i,j}e^0_{i,j})}{\sum_{i,j}\rho^0_{i,j}e^0_{i,j}}$ of the system when the operator $\mathscr{T}_Y(\Phi, Y)$ is defined with the non-diffusive scheme proposed in Section 3.4 or with the standard first order upwind scheme.

These numerical results show that the proposed 2D algorithm is accurate, stable and converges toward a good thermodynamic equilibrium when $t^n \to +\infty$. They also underline that the *entropic correction* is necessary to obtain the stability and the convergence of the algorithm when $t^n \to +\infty$ (compare Figs. 7 and 8). Moreover, they show that the relative mass and energy errors oscillate around a tiny constant during the transient regime: this property is directly connected to the non-diffusive property of the 2D interface capturing algorithm proposed in Section 3.4. For example, we see on Fig. 10 that these errors are not controlled during the transient regime when $\mathscr{T}_Y(\Phi, Y)$ is defined with a standard upwind scheme. We can also deduce from Fig. 6 that the thickness of the artificial mixture area is of the order of three cells: cf. also Section 4.6 for a more accurate estimation of this thickness.

4.5. Second test case: dilation of six bubbles on a 100×100 mesh

The topological changes obtained with the first test case are not important in the sense that the bubble remains circular and centered in Ω (compare Figs. 5 and 6). Of course, this is due to the symmetry of the flow and to the fact that the surface of the bubble is not disturbed by another bubble or by the boundary $\partial\Omega$. To study more important topological changes, we now define the initial temperature field with

$$\begin{aligned} T^0_{i,j} = 10 \times \Bigg\{ & 1 - 0.5\exp\left[-\frac{125}{4}\left((x_{i,j}-0.5)^2 + y^2_{i,j}\right)\right] - 0.75\exp\left[-\frac{125}{4}\left((x_{i,j}+0.5)^2 + y^2_{i,j}\right)\right] \\ & - 0.5\exp\left[-\frac{125}{4}\left(x^2_{i,j} + (y_{i,j}-0.48)^2\right)\right] - 0.8\exp\left[-\frac{125}{4}\left((x_{i,j}-0.3)^2 + (y_{i,j}+0.42)^2\right)\right] \\ & - \exp\left[-\frac{125}{4}\left(x^2_{i,j} + y^2_{i,j}\right)\right] - \exp\left[-\frac{125}{4}\left((x_{i,j}+0.48)^2 + (y_{i,j}-0.53)^2\right)\right] \Bigg\} + 2\times 10^{-2} \end{aligned} \tag{89}$$

and the initial mass fraction with

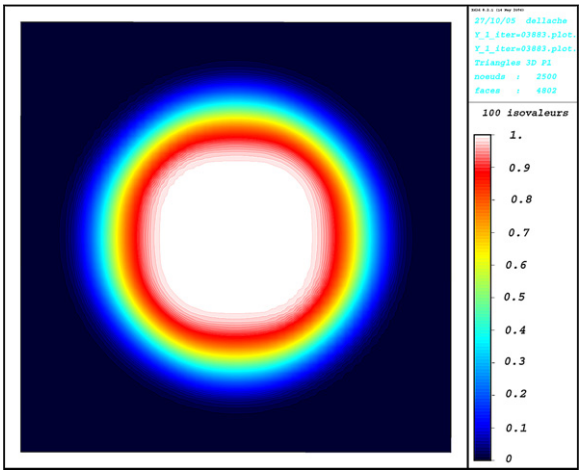

Fig. 9: Mass fraction $Y^n_{i,j}$ when $t^n = 300$.

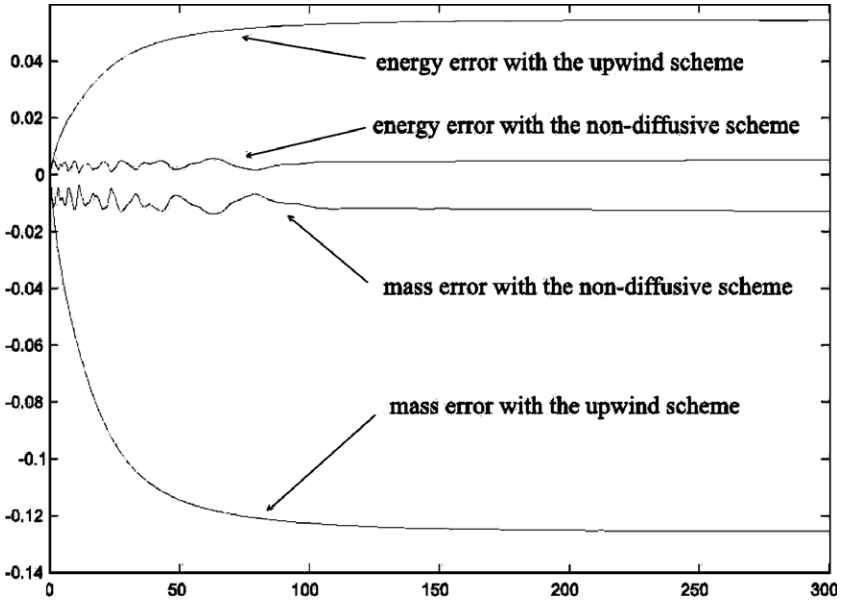

Fig. 10: Mass error of the bubble and energy error.

Fig. 9 and 10. $\mathscr{T}_Y(\Phi, Y)$ is defined with a first order upwind scheme (first test case).

$$Y^0_{i,j} = \begin{cases} 1 & \text{if } T^0_{i,j} < 7.5, \\ 0 & \text{if not.} \end{cases} \tag{90}$$

As for the first test case, the quantity 2×10^{-2} is added to impose $T^0_{i,j} > 0$ in Ω. Let us underline that this test case is hard: indeed, the initial temperature is close to zero at the center of two of the six bubbles and the initial temperature differences are large. This is also the case for the previous test case. Figs. 11 and 12 show the mass fractions $Y^0_{i,j}$ and $Y^n_{i,j}$ when $t^n = 100$ (which corresponds to $n \simeq 6300$). Figs. 13 and 14 show the temperature and the density at $y = 0$ when $t^n = 12.5$ and $t^n = 100$. Fig. 15 shows the pressure $P(t^n)/P^\infty$, the entropy $\mathscr{S}(t^n)/|\mathscr{S}^\infty|$ and the surface $S_1(t^n)/S_1^\infty$. Fig. 16 shows the relative mass and energy errors.

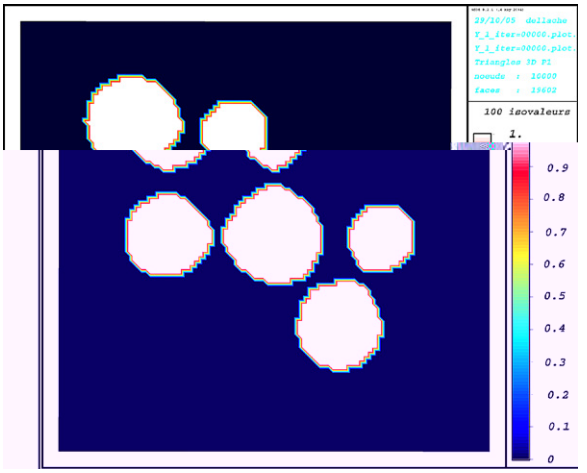

Fig. 11. initial mass fraction $Y^0_{i,j}$ (second test case).

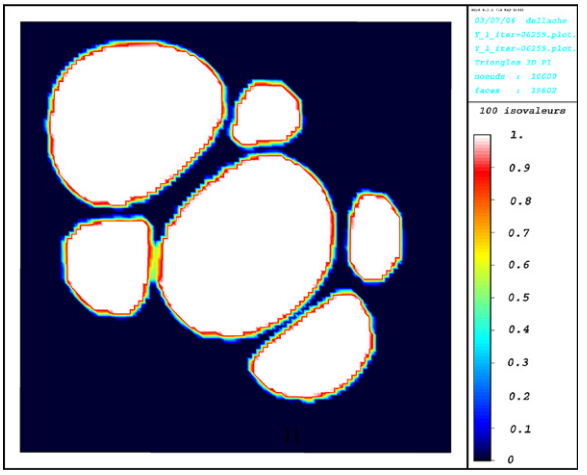

Fig. 12. mass fraction $Y^n_{i,j}$ when $t^n = 100$ (second test case).

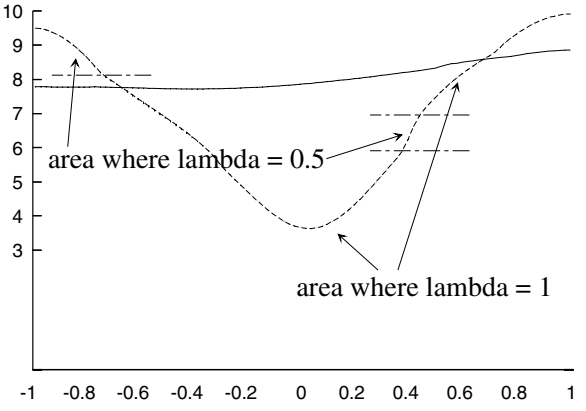

Fig. 13. $T^n_{i,j}$ for $y_{i,j} = 0$, $t^n = 12.5$ (dashed line) and $t^n = 100$ (second test case).

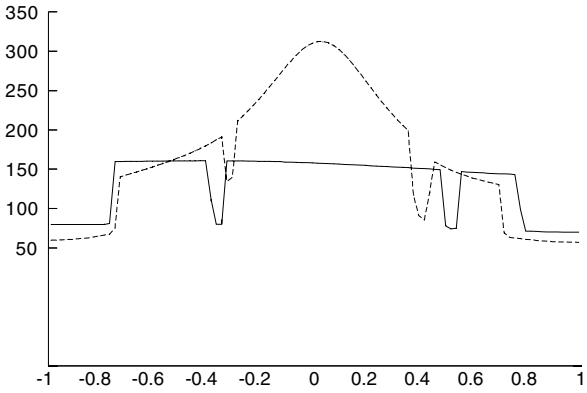

Fig. 14. $\rho_{i,j}^n$ for $y_{i,j} = 0$, $t^n = 12.5$ (dashed line) and $t^n = 100$ (second test case).

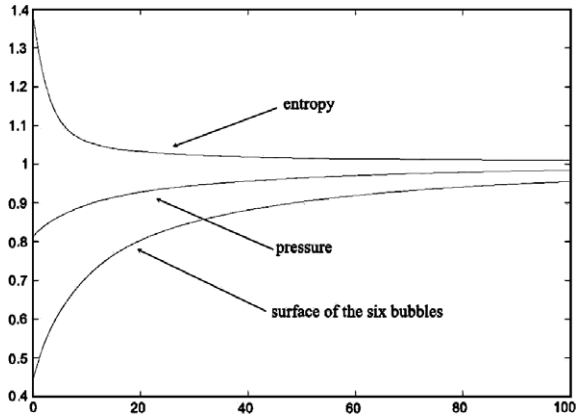

Fig. 15. $P(t)/P^\infty$, $\mathscr{S}(t)/\mid \mathscr{S}^\infty \mid$ and $S_1(t)/S_1^\infty$ (second test case).

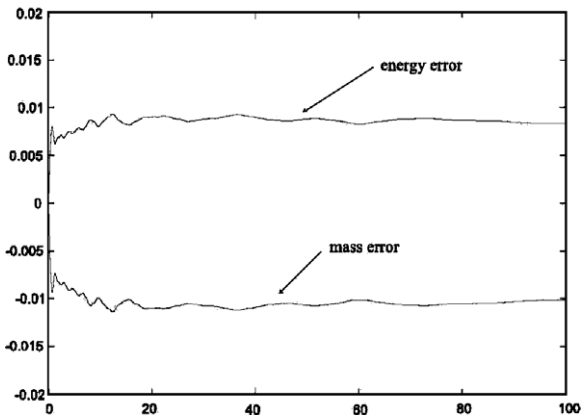

Fig. 16. Mass of the six bubbles and energy errors.

The initial data (89) and (90) allow to define six bubbles which are initially circular and close to each other (cf. Fig. 11). Since the initial temperature in each bubble is lower than the temperature outside the bubble, the volume of each bubble increases (i.e. dilation). This induces quasi contacts between the bubbles (and between one of the six bubbles and the boundary $\partial\Omega$): a consequence is that we obtain important deformations of the

initial circular topology. For example, two of the six bubbles are pinched by two bigger bubbles during the dilation making the surface of these two bubbles close to a "singular" surface: see Fig. 12. Fig. 13 shows that the discontinuity of the temperature gradient ∇T (induced by the fact that $\lambda_1 \neq \lambda_2$) is taken into account by the algorithm and that the temperature converges toward a constant. Fig. 14 shows that the discontinuity of the density field is well taken into account by the mixture model (26)–(28) of the DLMN-$\mathscr{M}$ system. The Fig. 15 confirms that the algorithm is stable and converges toward a good thermodynamic equilibrium when $t^n \to +\infty$. As for the first test case (cf. Fig. 8), we verify that there is no convergence when the *entropic correction* is not applied. Fig. 16 shows that the relative mass and energy errors oscillates, as for the first test case (cf. Fig. 10), around a tiny constant during the transient regime.

4.6. Convergence and estimation of the thickness of the artificial mixture area

We now study numerically the convergence of the 2D algorithm and the non-diffusive property of the 2D interface capturing algorithm.

- *Convergence:* Fig. 17 represents in logscales for three different meshes the absolute values of the mass and energy errors in function of Δx ($\Delta y = \Delta x$) at the time $t^n = 50$ in the case of the second test case. The three meshes are the following: 50×50 ($\Delta x = \Delta x_1$), 100×100 ($\Delta x = \Delta x_1/2$) and 200×200 ($\Delta x = \Delta x_1/4$). This figure shows that the algorithm is convergent and is a first order algorithm. Despite this first order, we now show that the interface capturing algorithm is precise through its non-diffusive property. Let us underline that we have already shown in Section 4.1 that the interface capturing algorithm is precise and can preserve the fine structure of the interface $\Sigma(t)$ in the case of the system (81) (see Figs. 1–4).
- *Non-diffusive property:* Let us define the quantity

$$v^n := \frac{1}{2\sqrt{\pi}\min(\Delta x, \Delta y)} \cdot \frac{S_\Omega - \sum_{i,j}(\delta_{1,Y^n_{i,j}} + \delta_{0,Y^n_{i,j}})\Delta x \Delta y}{\sqrt{\sum_{i,j} Y^n_{i,j} \Delta x \Delta y}} \tag{91}$$

($\delta_{a,b}$ is the Kronecker symbol). The quantity $v^n \times \min(\Delta x, \Delta y)$ is an estimation of the thickness of the artificial mixture area. The estimation (91) supposes that $\Omega_1(t^n)$ is always close to a circle for sake of simplicity, which is only true for the first test case (cf. Fig. 6). Fig. 18 represents v^n for the first test case when

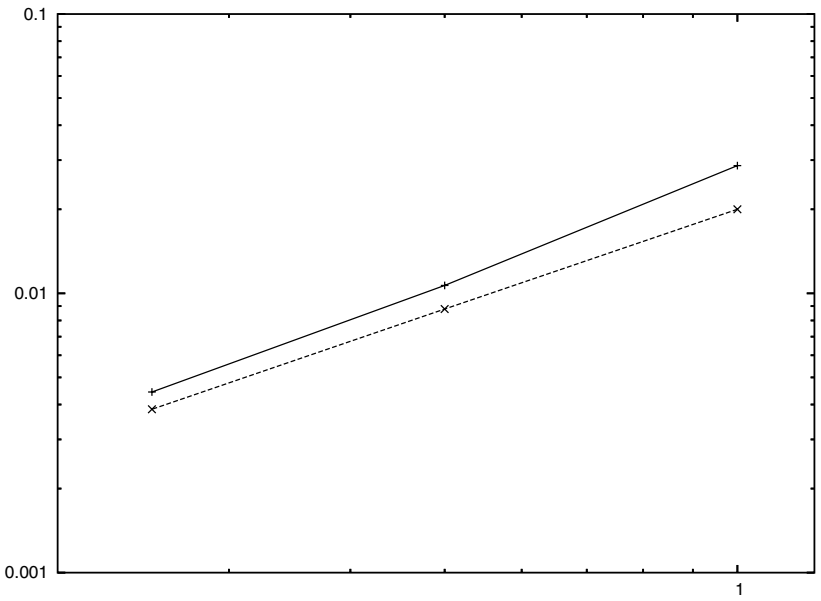

Fig. 17. Convergence of the scheme when $\Delta x \to 0$ (second test case).

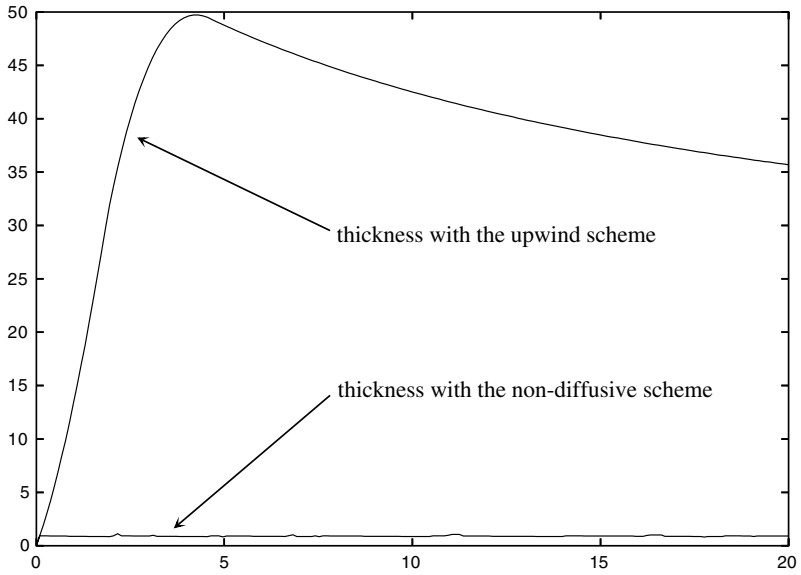

Fig. 18. Estimation of the thickness v^n of the artificial mixture area (first test case) (second test case).

$t^n \in [0, 20]$. It confirms that the order of the thickness of the mixture area is almost constant and lower than three cells during the transient regime. This figure shows also that this central property of our algorithm is not achieved when $\mathscr{T}_Y(\Phi, Y)$ is defined with a standard first order upwind scheme. The increasing of v^n is due to the numerical diffusion and the decreasing of v^n is due to a *bad* interaction of the artificial mixture area with the boundary $\partial\Omega$ during the transient regime, interaction which artificially compresses the circular geometry of the bubble (see also Fig. 9).

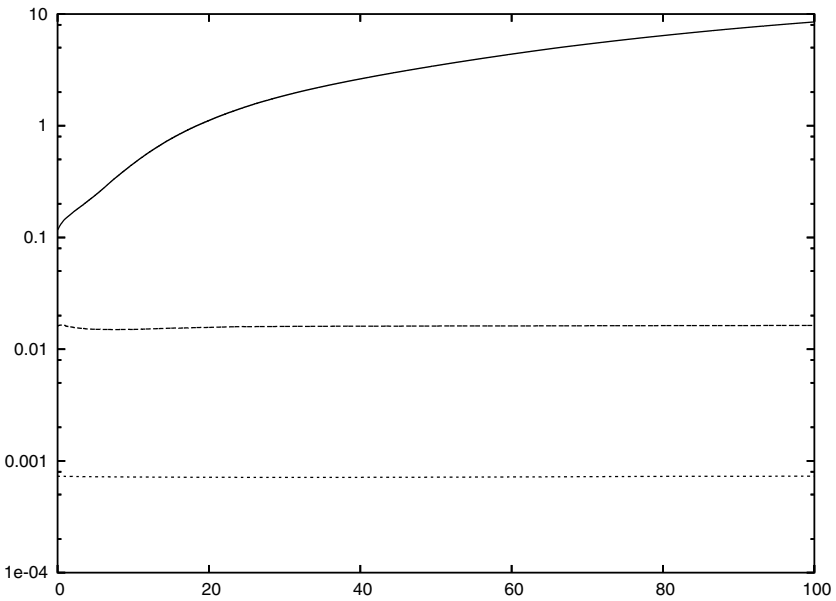

Fig. 19. $\Delta t_u(t^n)$, $\Delta t_{\mathcal{T}}(t^n)$ (dashed line) and $\Delta t_{ac}(t^n)$ (dotted lines) (second test case).

4.7. Study of the time step Δt

Let us recall that the time step Δt is defined with (79) and (80). The time steps Δt_u and Δt_T define, respectively, a time scale associated to the velocity field and a time scale associated to the heat conduction.

We represent in Fig. 19 for the second test case the quantities $\log_{10}\Delta t_u(t^n)$, $\log_{10}\Delta t_T(t^n)$ (dashed line) and $\log_{10}\Delta t_{ac}(t^n)$ (dotted line) where $\Delta t_{ac} = \frac{\Delta x}{\max_{i,j} c^n_{i,j}}$ is a time scale associated to the acoustic waves celerity. Fig. 19 shows that the time step Δt of our algorithm is always equal to Δt_T and that $\Delta t_T/\Delta t_u$ converges exponentially to zero when $t^n \to +\infty$. This is a consequence of the potential approximation of the DLMN system which does note take into account the dynamic part of the DLMN system by only focusing on the diphasic thermodynamic character of the DLMN system. By taking into account the momentum equation with a high gravity field for example, the time step Δt_u could be much lower. This figure shows also that $\Delta t_{ac}/\Delta t_u$ is always close to zero and that $\Delta t_{ac}/\Delta t \simeq 10^{-1}$ since $\Delta t = \Delta_T$. Thus, to diminish the CPU time i.e. to replace the constraint (79) by the constraint $\Delta t = \mathrm{CFL} \times \Delta t_u$, future works should study the implicitation of the temperature equation (38)(b). The linear implicit schemes

$$T^{n+1}_{i,j} = T^n_{i,j} + \Delta t \cdot \left[-\mathscr{T}_T(\Phi^n, T^{n+\theta_1})_{i,j} + \beta^n_{i,j} \left(\frac{\mathscr{P}'(Y^n, T^n, P^n)}{P^n} T^{n+\theta_2}_{i,j} + \frac{\widehat{\mathscr{D}}_T(Y^n, T^{n+\theta_3})_{i,j}}{\alpha^n_{i,j} P^n} \right) \right]$$

with $\theta_k \in \{0,1\}$ – the entropic correction (69)(a) (or (b)) in $\widehat{\mathscr{D}}_T$ being explicit – should be studied.

5. Conclusion

We have proposed a bidimensional (2D) algorithm for the simulation of the potential diphasic low Mach number (DLMN) system. Following the approach proposed in [20,31] for the numerical discretization of the diphasic compressible Euler system, we have built our algorithm by following a *two-steps approach*: in the first step, we have extended the DLMN system to the case of a mixture by defining the DLMN-$\mathscr{M}$ system through ad hoc closure laws modelling a mixture; in the second step, we have proposed an interface capturing algorithm based on the transport of an Heaviside function using the Després–Lagoutière's non-diffusive scheme [18,19,31]. The potential approximation of the DLMN system – which was deduced from an operators splitting – has been introduced to focus on the numerical difficulties coming from the diphasic *thermodynamic* character rather than from the diphasic *thermodynamic* + *dynamic* character of the DLMN system. This study has shown that when the initial temperature differences are large, it appears numerical instabilities which prevent the scheme to converge to a good thermodynamic equilibrium when the time goes to infinity. We have shown that these instabilities are due to the non-entropic character of the scheme. Thus, we have proposed an *entropic correction* to make entropic our algorithm. This entropic correction was inspired from numerical algorithms proposed in the field of kinetic equations [6,12]. It is important to note that, without this entropic correction, these numerical instabilities would also be present in the case of the no-potential DLMN system.

The 2D numerical results show that our 2D algorithm is *stable* and *accurate*. It is *stable* in the sense that it converges without any instabilities toward a discrete equilibrium when the time goes to infinity despite the fact that the equations of state and the thermal conductivities are not continuous functions and despite the large initial temperature differences. It is *accurate* in the sense that the thickness of the artificial mixture area is almost constant and lower than three cells during the transient regime and in the sense that the discrete equilibrium is closed to the theoretical discrete thermodynamic equilibrium. Let us underline that we do not use any numerical tuning to stabilize or to make more accurate our algorithm and that the 3D extension is natural.

Acknowledgments

We thank the *Service Fluides Numériques, Modélisation et* Études of the *Commissariat à l'*Énergie *Atomique* (Saclay, France) and the *Centre de Recherches Mathématiques* (Montréal, Canada) for their financial support.

References

[1] G. Allaire, S. Clerc, S. Kokh, A five-equation model for the numerical simulation of interfaces in two-phase flows, C. R. Acad. Sci., Paris, Série I, Math. 331 (12) (2000) 1017–1022.

[2] G. Allaire, S. Clerc, S. Kokh, A five-equation model for the simulation of interfaces between compressible fluids, J. Comput. Phys. 181 (2002) 577–616.

[3] F. Alouges, F. De Vuyst, G. Le Coq, E. Lorin, Un procédé de réduction de la diffusion numérique des schémas à différences de flux d'ordre un pour les systèmes hyperboliques non-linéaires, C. R. Acad. Sci., Paris, Série I, Math. 335 (7) (2002) 627–632.

[4] N. Al-Rawahi, B. Bunner, A. Esmaeeli, J. Han, Y.-J. Jan, D. Juric, S. Nas, W. Tauber, G. Tryggvason, A front-tracking method for the computations of multiphase flow, J. Comput. Phys. 169 (2001) 708–759.

[5] J.U. Brackbill, D.B. Kothe, C. Zemach, A continuum method for modeling surface tension, J. Comput. Phys. 100 (1992) 335–354.

[6] C. Buet, S. Dellacherie, R. Sentis, Numerical solution of an ionic Fokker–Planck equation with electronic temperature, SIAM Numer. Anal. 39 (4) (2001) 1219–1253.

[7] A.J. Chorin, A numerical method solving incompressible viscous flow problems, J. Comput. Phys. 2 (1967) 12–26.

[8] A.J. Chorin, Numerical solution of the Navier–Stokes equations, Math. Comput. 22 (1968) 745–762.

[9] A.J. Chorin, J.E. Mardsen, A Mathematical Introduction to Fluid Mechanics, Springer, Berlin, 1979.

[10] V. Daru, M.-C. Duluc, D. Juric, O. Le Maître, P. Le Quéré, Simulation numérique d'écoulements liquide-vapeur faiblement compressibles, in: Proceedings of the 17ème Congrès Français de Mécanique, 2005.

[11] J.M. Delhaye, E. Hervieu, M. Ishii, J.M. Le Corre, Benchmarking and improvements of measurements techniques for local time-averaged two-phase flow parameters, in: Fourth International Conference on Multiphase Flows (ICMF 2001), New-Orleans, USA, 2001.

[12] S. Dellacherie, Sur un schéma numérique semi-discret appliqué à un opérateur de Fokker–Planck isotrope, C. R. Acad. Sci., Paris, Série I, Math. 328 (1999) 1219–1224.

[13] S. Dellacherie, On relaxation schemes for the multicomponent Euler system, Math. Modelling Numer. Anal. 37 (6) (2003) 909–936.

[14] S. Dellacherie, On a diphasic low Mach number system, Math. Modelling Numer. Anal. 39 (3) (2005) 487–514.

[15] S. Dellacherie, O. Lafitte, Existence et unicité d'une solution classique à un modèle abstrait de vibration de bulles de type hyperbolique-elliptique, Publication of the Centre de Recherches Mathématiques of Montréal (Canada), CRM-3200, 2005.

[16] S. Dellacherie, O. Lafitte, Solutions autosemblables pour des modèles avec conductivité thermique, Publication of the Centre de Recherches Mathématiques of Montréal (Canada), CRM-3207, 2005.

[17] S. Dellacherie, A. Vincent, Zero Mach number diphasic equations for the simulation of water-vapor high pressure flows, in: Proceedings of the 11th Conference of the CFD Society of Canada, Vancouver, 2003, pp. 248–255.

[18] B. Després, F. Lagoutière, Un schéma non-linéaire anti-dissipatif pour l'équation d'advection linéaire, C. R. Acad. Sci., Paris, Série I, Math. 328 (1999) 939–944.

[19] B. Després, F. Lagoutière, Contact discontinuity capturing schemes for linear advection and compressible gas dynamics, J. Sci. Comput. 16 (4) (2001) 479–524.

[20] B. Després, F. Lagoutière, Numerical resolution of a two-component compressible fluid model with interfaces, Prog. Comput. Fluid Dyn. (to appear).

[21] P. Embid, Well-posedness of the nonlinear equations for zero Mach number combustion, Commun. Partial Differential Equations 12 (11) (1987) 1227–1283.

[22] P. Embid, On the reactive and non-diffusive equations for zero Mach number flow, Commun. Partial Differential Equations 14 (8,9) (1989) 1249–1281.

[23] M. Fulgosi, D. Lakehal, M. Meier, Interface tracking towards the direct numerical simulation of heat and mass transfer in multiphase flows, Int. J. Heat Fluid Flow 23 (2002) 242–257.

[24] E. Godlewsky, P.A. Raviart, Numerical approximation of hyperbolic systems of conservation lawsApplied Mathematical Sciences, vol. 118, Springer, Berlin, 1996.

[25] D. Gueyffier, J. Li, A. Nadim, R. Scardovelli, S. Zaleski, Volume-of-fluid interface tracking with smoothed surface stress methods for three-dimensional flows, J. Comput. Phys. 152 (1999) 423–456.

[26] F.H. Harlow, J.E. Welch, Numerical calculation of time-dependent viscous incompressible flow of fluid with free surface, Phys. Fluids 8 (12) (1965) 2182–2189.

[27] D. Juric, S. Shin, Modeling three-dimensional multiphase flow using a level contour reconstruction method for front tracking without connectivity, J. Comput. Phys. 180 (2002) 427–470.

[28] D. Juric, G. Tryggvason, Computations of boiling flows, Int. J. Multiphase Flow 24 (3) (1998) 387–410.

[29] S. Kokh, Aspects numériques et théoriques de la modélisation des écoulements diphasiques compressibles par des méthodes de capture d'interface, Ph.D. Thesis of Paris VI University, 2001.

[30] A. Kumbaro, H. Paillère, I. Toumi, C. Viozat, Comparison of low Mach number models for natural convection problems, Heat Mass Transfer 36 (2000) 567–573.

[31] F. Lagoutière, Modélisation mathématique et résolution numérique de problème de fluides compressibles à plusieurs constituants, Ph.D. Thesis of Paris VI University, 2000.

[32] K.G. Lamb, A. Majda, Simplified equations for low Mach number combustion with strong heat release, in: Dynamical Issues in Combustion TheoryIMA Volumes in Mathematics and its Applications, vol. 35, Springer, Berlin, 1991, pp. 167–211.

[33] A. Majda, Equations for low mach number combustion, Center of Pure and Applied Mathematics, University of California at Berkeley, Report No. 112, 1982.

[34] A. Majda, Compressible fluid flow and systems of conservation laws in several space variables, Applied Mathematical Sciences Series, vol. 53, Springer, New York, 1984 (Chapter 2).
[35] A. Majda, J.A. Sethian, The derivation and numerical solution of the equations for zero Mach number combustion, Combust. Sci. Tech. 42 (1985) 185–205.
[36] W. Mulder, S. Osher, J.A. Sethian, Computing interface motion in compressible gas dynamics, J. Comput. Phys. 100 (1992) 209–228.
[37] P.J. O'Rourke, The acoustic mode in numerical calculations of subsonic combustion, in: P. Clavin, B. Larrouturou, P. Pelce (Eds.), Combustion and Nonlinear Phenomena, Les Éditions de Physique, 1986, pp. 229–241.
[38] S. Osher, P. Smereka, M. Sussman, A level set approach for computing solutions to incompressible two-phase flow, J. Comput. Phys. 114 (1994) 146–159.
[39] S. Paolucci, On the filtering of sound from the Navier–Stokes equations, Sandia National Laboratories Report, SAND82-8257, 1982.
[40] G. Russo, P. Smereka, A remark on computing distance functions, J. Comput. Phys. 163 (2000) 51–67.
[41] J.A. Sethian, Level set methods, Cambridge Monographs on Applied and Computational Mathematics, Cambridge University Press, Cambridge, 1996.
[42] G.A. Sivashinsky, Hydrodynamic theory of flame propagation in an enclosed volume, Acta Astronautica, vol. 6, Pergamon Press, 1979, pp. 631–645.
[43] P.K. Sweby, High resolution schemes using flux limiters for hyperbolic conservation laws, SIAM J. Numer. Anal. 21 (1984) 995–1011.
[44] E.F. Toro, Riemann Solvers and Numerical Methods for Fluid Dynamics. A Practical Introduction, second ed., Springer, Berlin, 1999.
[45] G. Tryggvasson, S.O. Unverdi, A front-tracking method for viscous, incompressible, multi-fluid flows, J. Comput. Phys. 100 (1992) 25–37.
[46] S.W.J. Welch, J. Wilson, A volume of fluid based method for fluid flows with phase change, J. Comput. Phys. 160 (2000) 662–682.